

**QUANTUM MONTE CARLO STUDY OF WEAKLY INTERACTING MANY-
ELECTRON SYSTEMS**

by

Jiawei Xu

B.S. in Chemistry, University of Science and Technology of China, 2002

M.S. in Chemistry, University of Science and Technology of China, 2002

Submitted to the Graduate Faculty of
the Dietrich School of Art and Science in partial fulfillment
of the requirements for the degree of
Doctor of Philosophy in Physical Chemistry

University of Pittsburgh

2012

UNIVERSITY OF PITTSBURGH
THE DIETRICH SCHOOL OF ART AND SCIENCE

This dissertation was presented

by

Jiawei Xu

It was defended on

August 03, 2012

and approved by

Kenneth Jordan, PhD, Distinguished Professor

Karl Johnson, PhD, Professor

Lillian Chong, PhD, Associate Professor

Haitao Liu, PhD, Assistant Professor

Dissertation Advisor: Kenneth Jordan, PhD, Distinguished Professor

Copyright © by Jiawei Xu

2012

QUANTUM MONTE CARLO STUDY OF WEAKLY INTERACTING MANY-ELECTRON SYSTEMS

Jiawei Xu, PhD

University of Pittsburgh, 2012

Quantum Monte Carlo (QMC) methods are playing an increasingly important role for providing benchmark results for testing more approximate electronic structure and force field methods. Two particular variants of QMC, the variational Monte Carlo (VMC) and diffusion Monte Carlo (DMC) methods, have been applied to study the many-electron systems. All-electron calculations using QMC methods are performed to study the ground-state energy of the Be atom with single-determinant and multi-determinant trial functions, the binding energy of the water dimer, and the binding energy of the water-benzene complex. All of the DMC results achieve good agreement with high level *ab initio* methods and experiments. The QMC method with pseudopotentials is used to calculate the electron binding energies of two forms of $(\text{H}_2\text{O})_6$. It is found that the DMC method, when using either Hartree-Fock or density functional theory trial functions, gives electron binding energies in excellent agreement with the results of large basis set CCSD(T) calculations. Pseudopotential QMC methods are also used to study the interactions of the water-benzene, water-anthracene, and water-coronene complexes. The dissociation energies of water-acene complexes of the DMC calculations agree with several other high level quantum calculations. Localized orbitals represented as spline functions are used to reduce the computational cost of the calculations for larger water-acene complexes. The prospects of using this approach to determine the interaction energy between water and graphite are discussed. In addition, we introduce correlation-consistent Gaussian-type orbital basis sets for use with the

Casino Dirac-Fock pseudopotentials. These basis sets give low variances in VMC calculations and lead to significantly improved convergence compared to non-optimized basis sets in DMC calculations. We also examine the performance of two methods, the locality approximation (LA) and T-move, that have been designed for dealing with the problems associated with the use of non-local pseudopotentials in quantum Monte Carlo calculations. The two approaches give binding energies of water dimer that agree within the statistical errors. However, the convergence behavior of the DMC calculations is better behaved when using the T-move approach.

TABLE OF CONTENTS

PREFACE	XIII
1.0 INTRODUCTION	1
2.0 THE QUANTUM MONTE CARLO METHOD	7
2.1 INTRODUCTION	7
2.2 THE METROPOLIS ALGORITHM	8
2.3 VARIATIONAL MONTE CARLO	11
2.4 DIFFUSION MONTE CARLO	14
2.4.1 Introduction	14
2.4.2 The Green's Function Propagator	15
2.4.3 The Short Time Approximation	16
2.4.4 The Simple Sampling	17
2.4.5 Importance Sampling	20
2.4.6 Fixed Node Approximation	21
2.5 TRIAL WAVE FUNCTION	23
3.0 THE QMC STUDY OF THE BE ATOM	26
3.1 INTRODUCTION	26
3.2 COMPUTATIONAL DETAILS	26
3.3 RESULTS	28

4.0	THE QMC STUDY OF WATER DIMER.....	31
4.1	INTRODUCTION	31
4.2	COMPUTATIONAL DETAILS	32
4.3	RESULTS	34
5.0	THE QMC STUDY OF WATER CLUSTER ANION	37
5.1	INTRODUCTION	37
5.2	COMPUTATIONAL DETAILS	38
5.3	RESULTS.....	40
6.0	THE QMC STUDY OF THE WATER-ACENE SYSTEMS.....	44
6.1	INTRODUCTION	44
6.2	THE QMC STUDY OF THE WATER-BENZENE COMPLEX WITH ALL- ELECTRON TRIAL FUNCTIONS	45
6.2.1	Introduction	45
6.2.2	Computational details	47
6.2.3	Results.....	48
6.3	THE QMC STUDY OF THE WATER-ANTHRACENE COMPLEX WITH PSEUDOPOTENTIAL	49
6.3.1	Introduction	49
6.3.2	Computational details	51
6.3.3	Results.....	52
6.4	THE QMC STUDY OF LARGE WATER-ACENE SYSTEMS USING LOCALIZED ORBITALS	52
6.4.1	Introduction	52

6.4.2	Computational details and results.....	54
6.5	THE QMC STUDY OF THE WATER-BENZENE AND WATER-CORONENE COMPLEX WITH PSEUDOPOTENTIAL	55
6.5.1	Introduction	55
6.5.2	Computational Details.....	57
6.5.3	Results.....	61
6.5.4	Conclusions.....	67
7.0	NEW GAUSSIAN BASIS SETS FOR QUANTUM MONTE CARLO CALCULATIONS	69
7.1	INTRODUCTION	69
7.2	VMC CALCULATIONS.....	70
7.3	DMC CALCULATIONS.....	78
7.4	CONCLUSIONS.....	85
8.0	SUMMARY	86
	REFERENCE.....	90

LIST OF TABLES

Table 1.1 Comparison of methods for C ₁₀	5
Table 3.1 Total energy of the Be atom calculated with different <i>ab initio</i> methods, and the experimental result.....	28
Table 3.2 DMC energy of the Be atom calculated with different Cas trial functions.	30
Table 4.1 Coordinates of the water dimer in Å.....	34
Table 4.2 Total energies of the water monomer from various <i>ab initio</i> methods.....	35
Table 4.3 Equilibrium dissociation energies of the water dimer from various <i>ab initio</i> methods and the experiment.....	35
Table 5.1 Total energies (au) of the neutral and anion of A.....	41
Table 5.2 Total energies (au) of the neutral and anion of B	41
Table 5.3 Electron binding energies (EBE) (ev) of species A and B	43
Table 6.1 Equilibrium Dissociation Energy of the water-benzene system from various <i>ab initio</i> methods.....	47
Table 6.2 Equilibrium Dissociation Energy of the water-anthracene system.....	51
Table 6.3 Total energy and binding energy of the water-benzene complex.....	62
Table 6.4 Binding energy of the water-coronene complex.....	65
Table 6.5 Binding energies (kcal/mol) of water-benzene, water-coronene, and water-graphene.....	66

Table 7.1 VMC energies and variances for the water monomer using the Casino Dirac-Fock pseudopotential on all atoms ^a	71
Table 7.2 aug-cc-pVXZ basis sets for oxygen in Gaussian09 format	72
Table 7.3 aug-cc-pVXZ basis sets for hydrogen in Gaussian09 format	74
Table 7.4 aug-cc-pVXZ basis sets for carbon in Gaussian09 format	75
Table 7.5 VMC energies and variances for the water monomer ^a	77
Table 7.6 Calculated binding energy of water dimer	83

LIST OF FIGURES

Figure 2.1 The process of the Variational Monte Carlo (VMC) calculation	13
Figure 4.1 The equilibrium structure of the water dimer	33
Figure 5.1 Geometrical structures of the A and B forms of $(\text{H}_2\text{O})_6^-$	39
Figure 6.1 MP2-optimized global minimum structure of the water-benzene complex	46
Figure 6.2 Time-step dependence of the equilibrium dissociation energy of the water-benzene system for the DMC/ HF-6-311++G** calculations	49
Figure 6.3 DMC energy of the water-anthracene complex as a function of the time step	50
Figure 6.4 MP2-optimized structure of the water-anthracene complex	51
Figure 6.5 Computational cost of the DMC calculations for acene molecules as a function of the system size	54
Figure 6.6 Geometrical structures of the water-benzene and water-coronene.....	58
Figure 6.7 Binding energy of water-benzene from DMC calculations using strategies S1 and S2 and basis sets B and C.....	63
Figure 6.8 Binding energy of water-coronene from DMC calculations using S1 and S2 strategies	65
Figure 7.1 DMC energy of the water molecule with different trial functions	78

Figure 7.2 DMC energies of the water dimer obtained using different basis sets for representing the orbitals, different choices of Jastrow factors, and two strategies for dealing with the problems posed by non-local pseudopotentials 81

Figure 7.3 Energies of the water dimer on an expanded scale, from DMC calculations using the aug-cc-pVTZ (CDF) basis set..... 82

Figure 7.4 Binding energies of water dimer with two different trial functions and strategies 84

PREFACE

My deepest gratitude is to my advisor, Professor Kenneth D. Jordan for his guidance, patience, understanding and supports during my graduate studies at the University of Pittsburgh. Much of my knowledge in the quantum mechanics theory and computational science came from this precious spell of time. Ken's always kind and patient mentorship and his incise way of approaching the fundamental problems are paramount for me to achieve my long-term professional goals!

I am indebted to the faculty members in the Eberly Hall, Professor Rob Coalson, Professor Wissam Al-Saidi, Professor Geoffrey Hutchison and Professor Lillian Chong for the teachings and their kind suggestions to my research!

I would like to thank my committee members: Prof. Karl Johnson, Prof. Lillian Chong, and Prof. Haitao Liu for any advice while preparing this document.

I have benefited enormously from discussions with many former Jordan group members, Professor Thomas Sommerfeld, Dr. Hao Jiang, Dr. Jun Cui, Dr. Albert Defusco, Dr. Tae Hoon Choi, Dr. Haitao Liu, Dr. Daniel Schofield, and the current group members! Special thanks go to Dr. Revati Kumar and Dr. Fangfang Wang for many helpful discussions on the water models.

I am also thankful to Dr. Richard Christie and the SAM team for the many years' assistance on the carrying out calculations!

I would like to thank the Department of Chemistry at the University of Pittsburgh especially, Elaine Springel and Fran Nagy, for providing us such an easy studying environment!

I would also like to extend thanks to Dr. Kirk Peterson, Dr. Dario Alfè, Dr. Richard Needs, Dr. Mike Towler and Dr. Neil Drummond, for their kind help and suggestions in my research.

Finally, I owe my greatest debts to my family. I thank my parents for their support and guidance in my life. I thank my beloved wife, Haixia, who shares my burdens and my joys. This dissertation is equally her achievement. For me, it is she who makes all things possible.

1.0 INTRODUCTION

During the past few decades, the *ab initio* quantum methods have been widely employed and dramatically improved in fields such as physics, chemistry, biochemistry, and material science and technology. With the help of the improvement of the computer's performance, the *ab initio* methods are not only applied to study small atomic and molecular systems, but also to larger systems, such as amino acids¹, proteins², and nanostructures³.

Carbon nanotubes (CNTs) have attracted considerable attention in recent years through their use in biosensor technology and other applications.⁴ The interest in the interaction of water with CNTs or graphite has also been growing, and the water- CNTs/graphite systems have been a subject of a number of fundamental studies aimed at exploring the structural and phase behavior of water at the nanometer scale⁵. For instance, it is interesting to study the behavior of water, as the preferred solvent for many applications, in an environment in which CNTs function as very small chemical reaction chambers, or “nanoreactors”⁶. Another example is the well-known effect of the environmental humidity on the friction and wear of graphitic carbons⁷, which is at variance with the common view that graphite is hydrophobic⁸.

Water can interact with acene molecules in several ways. Both H atoms and the O nonpaired electrons in H₂O can participate in forming bonds between molecules. Most acene compounds are immiscible in water, which indicates that the magnitudes of the interactions between water and aromatic molecules are very weak.

Research on water clusters plays a vital role in understanding the connection between the gas phase water molecular aggregates and the macroscopic condensed phase of water and allowing us to isolate particular hydrogen-bonded morphologies and then to predict how these networked “supermolecules” adapt and rearrange when exposed to different chemical and physical environments. Water cluster anions provide a model system to unravel how hydrogen-bonded water network deforms to accommodate the excess electron⁹ and help in understanding the free electron hydration at a molecular level. The interactions between water molecules in water clusters, and between the excess electron and water cluster are all weak noncovalent interactions.

These weak noncovalent interactions, such as van der Waals (vdW) dispersion interaction, possess a key role in many interesting areas of physics, chemistry, and biology. Their respective strengths determine the melting and boiling points as well as solvation energies and the conformation of large biomolecules.

However, how to describe these interactions accurately is a big challenge for *ab initio* electronic structure theories. One major problem in this study is the failure of both Hartree-Fock and traditional density functional theory (DFT) methods to treat long-range dispersion interactions (van der Waals)¹⁰, which are significant in this kind of system⁶. Due to the relatively low computational scaling (about N^3) of the algorithm (and efforts to develop linear scaling implementations are well underway), DFT methods are widely applied, such as in condensed matter systems¹¹, the modeling of molecular interactions with carbon interactions^{12,13}, and many other fields¹⁴. However, this method has a general drawback to describe long range correlations that are responsible for dispersive forces.¹⁵⁻¹⁷ Although there has been a lot of interest and effort in this DFT problem for dispersion interaction^{18,19}, such as introducing empirical long-range, $C_6 \cdot$

R^{-6} corrections, to standard functionals describing the dispersion part²⁰, there is no satisfactory solution as of yet.

Other methods that are more time consuming than DFT, such as 2nd order Møller-Plesset perturbation theory (MP2), can be used to treat this kind of systems in which dispersion interactions are important. Feller and Jordan have successfully applied MP2 in calculating water-graphite interacting systems by employing a cluster model of graphite⁶. However, MP2 is a more expensive way than DFT in CPU time, disk/memory requirements, and computational scaling (about N^5)²¹. Furthermore, there are several other issues arising when using MP2 to study water-CNTs/graphite systems. The first one is the basis set superposition error (BSSE), which arises from the incompleteness of the basis set, and leads to overestimation of binding energies and inaccurate molecular geometries. This kind of error can be corrected for, by either increasing the basis set size or employing the counterpoise correction methods. However, both of them are computationally demanding, and difficult to employ for large systems. In addition to BSSE, linear dependency occurs when an eigenvalue of the overlap matrix approaches zero and impedes the application of Gaussian basis sets with diffuse functions in studying large and complex systems with acene rings⁶. It introduces numerical errors and results in severe convergence problems in calculations²². While linear dependence can be overcome by projecting out or deleting functions in the basis set, such a removal of functions can lead to an overestimation in the interaction energy⁶.

In a certain sense the quantum Monte Carlo (QMC) method appears like a natural choice to overcoming the above problems. QMC has been developed to calculate the properties of assemblies of interacting quantum particles with high level of accuracy for decades. Two particular variants of QMC are in relatively common use, namely variational Monte Carlo

(VMC) and diffusion Monte Carlo (DMC). VMC is designed to sample a trial wave function, which is a reasonably good approximation of the true ground-state wave function, and calculate the expectation value of the Hamiltonian using Monte Carlo numerical integration. Its accuracy is limited by the necessity of guessing the functional form of the trial wave function, and there is no known way to systematically improve it all the way to the exact non-relativistic limit. Therefore, it is mainly used to provide the optimized trial wave function required as an importance sampling function to the much more powerful DMC technique. DMC is a stochastic projector method for solving the imaginary-time many-body Schrödinger equation. It is quite different from the conventional *ab initio* quantum chemistry methods, such as HF and DFT, which calculate the ground electronic state by a variational minimization of the expectation value of the energy. In principle, DMC is an exact method: inaccuracies are introduced only as a result of the antisymmetry problem and insufficient sampling in the Monte Carlo simulation. It can treat dispersion interactions accurately and, as it is not limited to describing the molecular orbitals with Gaussian basis sets, DMC does not run into BSSE or linear dependency problems.

Another attractive feature of DMC is the scaling behavior of the necessary computational effort with the system size. DMC scales as about N^3 ,²³ which is favorable when compared with other accurate methods correlated wave functions, such as Coupled Cluster Singles and Doubles (Triples) (CCSD(T)) method scaling as about N^7 . Foulkes²³ et al. provided a comparison of different methods for C₁₀. (see Table 1.1) DMC calculations was both more accurate and less time consuming than CCSD(T) with a b-311G* basis set, which is the largest affordable in CCSD(T) for C₁₀.

Table 1.1 Comparison of methods for C_{10} .

Method	E_{corr} ^a	E_{bind} ^b % errors	Scaling with # electrons	Total time ^d for C_{10}
HF ^c	0	≈ 50%	N^4	14
LDA	N/A	15-25 %	N^3	1
VMC	≈ 85%	2-10 %	$N^3 + \epsilon N^{4c}$	16
DMC	≈ 95%	1-4 %	$N^3 + \epsilon N^{4c}$	300
CCSD(T) ^e	≈ 75%	10-15 %	N^7	1500

a. $E_{corr} = E_{exact} - E_{HF}$ refers to the correlation energy.

b. E_{bind} is the binding energy.

c. $\epsilon \approx 10^{-4}$.

d. Times are given relative to the LDA timing.

e. With a b-311G* basis set, which is the largest affordable in CCSD(T) for C_{10} .

The third advantage of DMC is that the algorithm is inherently parallel, and thus the codes are easily adapted to a broad definition of parallel computers (encompassing machines with hundreds/thousands of CPU's, networked workstations, and multiprocessor workstations, etc.), and scale well with the number of processors. For example, the CASINO code, which was used in our VMC and DMC calculations, runs with a 99% parallel efficiency and achieves almost linear scaling on as many as 512 processors²⁴. Furthermore, the requirement of the memory and disk in DMC calculation is also modest even for relatively large systems²⁵.

In recent years, there has been more improvement in the computational scaling of DMC. Two different groups using the CASINO code, Williamson et al.²⁶ and Alfè and Gillan²⁷, developed a linear-scaling DMC algorithm, in which localized orbitals instead of the delocalized

single-particle orbitals are applied in the evaluation of the orbitals in the Slater determinants. This approach has been tested to be extremely effective in some cases.

For these reasons, QMC seems to be an accurate method available to study the many-electron problems, especially for the large weak interacting systems, such as the water-CNTs/graphite complexes.

2.0 THE QUANTUM MONTE CARLO METHOD

2.1 INTRODUCTION

The quantum Monte Carlo (QMC) method is a powerful approach for accurate solution of the many-electron Schrödinger equation. It imposes the use of random sampling, which is an efficient way to do numerical integrations of expressions involving wave functions in many dimensions, to solve the many-body Schrödinger equation which describes the electrons in the atomic or bulk materials. This makes it possible to build up statistical estimates of the ground state properties of the system without solving the Schrödinger equation explicitly.

There are different QMC methods, but only two types are concentrated in this document: variational quantum Monte Carlo (VMC)²⁸ and diffusion quantum Monte Carlo (DMC)²⁹⁻³¹. In the VMC method expectation values are calculated via Monte Carlo integration over the N -dimensional space of the electron coordinates. It is the simplest but least accurate. The DMC method is more complex but in principle generates exact solutions of the many-electron Schrödinger equation. In practice, the only errors present in a DMC calculation are due to the short time approximation and an approximation to the exact form of the nodal surface of the ground state wave function. Other quantum Monte Carlo methods, such as auxiliary-field QMC³² and path-integral QMC³³, may also be used to study interacting many-electron systems. However, they will not be discussed here.

2.2 THE METROPOLIS ALGORITHM

When using the QMC method to solve the many-electron Schrödinger equation, it is necessary to evaluate multidimensional integrals by sampling complicated probability distributions in high-dimensional spaces. However, it is complicated and difficult to sample the distributions directly because the normalizations of these distributions are always unknown. The Metropolis algorithm³⁴ is the most widely used algorithm that allows an arbitrarily complex distribution to be sampled in a straightforward way without knowledge of its normalization.

In the QMC method, each phase space point is a vector, $R = \{r_1, r_2, \dots, r_{N-1}, r_N\}$, in the $3N$ dimensional space of the position coordinates of all the N electrons. The sequence of phase space points provides a statistical representation of the ground state of the system. A statistical picture of the overall system of electrons and nuclei can be built up by moving the electrons around to cover all possible positions and hence all possible states of the system. As the electrons moving around, physical quantities such as the total energy, and polarization, *etc.*, which are associated with the instantaneous state of the electron configuration, can be tracked at the same time. Moreover, the sequence of individual samples of these quantities can be combined to arrive at average values which describe the quantum mechanical state of the system. This is the fundamental idea behind the Monte Carlo method, and the Metropolis algorithm is used to generate the sequence of different states to sample physical quantities such as the total energy efficiently. Many random numbers are used to generate the sequence of states, which are collectively called “a random walk”. And these random numbers are called walkers.

In a random walk with the Metropolis algorithm, the sampling is most easily accomplished if the points R form a Markov chain, which has two properties: 1. Each point on the walk belongs to a finite set $\{R_0, R_1, \dots, R_n, \dots\}$ called a phase space. 2. The position of each point in the chain depends only on the position of the preceding point and lies close to it in the phase space. The Metropolis algorithm generates the sequence of sampling points R_m by moving a single walker according to the following rules:

- (1) Generate a walker at a random position R_0 .
- (2) Move this walker from R_0 to a new position R_1 chosen from some transition probability T_{10} (from R_0 to R_1).
- (3) Accept or reject the trial move from R_0 to R_1 with a probability A_{01}

$$A(R_1 \leftarrow R_0) = \text{Min}\left(1, \frac{T(R_0 \leftarrow R_1)P(R_1)}{T(R_1 \leftarrow R_0)P(R_0)}\right) \quad 2.1$$

$P(R)$ is the probability of the state R . If the trial move is accepted, the point R_1 becomes the next point on the walk; if the trial move is rejected, the point R_0 becomes the next point on the walk. If $P(R)$ is high, most trial moves away from R will be rejected and the point R may occur many times in the set of points making up the random walk.

- (4) Return to step (2) and repeat. Finally, we can obtain a sampled distribution according to the probability $P(R)$.

To understand how this algorithm works, we consider a large ensemble of walkers with v_i and v_j as the populations of walkers at position R_i and R_j , respectively. If the density probability $P_j < P_i$, then the average number of walkers attempting a move from R_j to R_i will be $v_j T_{ij}$, in which T_{ij} is the transition probability as above. These trial moves will be accepted with acceptance ratio, A_{ij} . Similarly, from R_i to R_j the average number moving is $v_i T_{ji} A_{ji}$. The net increase in population at point R_j from point R_i is therefore

$$\delta v_j = T_{ji}A_{ji}v_i - T_{ij}A_{ij}v_j \quad 2.2$$

When the walk equilibrates, the average net population changes at any point must be zero. Thus, at equilibrium $\delta v_j = 0$, and from Eq. 2.2 we require,

$$T_{ji}A_{ji}v_i = T_{ij}A_{ij}v_j \quad 2.3$$

This can be rewritten as

$$\frac{v_j}{v_i} = \frac{T_{ji}A_{ji}}{T_{ij}A_{ij}} \quad 2.4$$

At equilibrium we know that $v_j / v_i = P_j / P_i$; therefore the acceptance ratio A must satisfy

$$\frac{A_{ji}}{A_{ij}} = \frac{P_j T_{ij}}{P_i T_{ji}} \quad 2.5$$

Equation 2.5 is called the detailed balance condition. It ensures that in the ensemble the ratio of the population is the ratio of the P .

A good choice for A to satisfy the detailed balance condition is

$$A_{ji} = \text{Min}\left(1, \frac{T_{ij}P_j}{T_{ji}P_i}\right) \quad 2.6$$

Therefore, at equilibrium the ratio of the population is proportional to ratio of the P . A rigorous derivation of this result is given by Feller³⁵.

Although the Metropolis algorithm has been widely used in different kinds of areas, it was Metropolis himself who first applied this algorithm to the quantum many-body problem in 1953³⁴. This work provided the base from which the modern variational and diffusion quantum Monte Carlo methods have developed.

2.3 VARIATIONAL MONTE CARLO

The variational method is a powerful approach for finding approximate solutions of the electronic Schrödinger equation³⁶. According to the variational principle, the expectation value of the energy of a trial wave function Ψ_T , given by

$$E[\Psi_T] = \frac{\langle \Psi_T^* | H | \Psi_T \rangle}{\langle \Psi_T^* | \Psi_T \rangle} \geq E_0 \quad 2.7$$

will be a minimum for the exact ground state wave function. For bound electronic states, Ψ_T may be assumed to be real, so Ψ_T is assumed to be equal to its complex conjugate Ψ_T^* . The functional $E[\Psi_T]$ thus provides an upper bound to the exact ground state energy. Generally, it is difficult to solve the integrals of a trial wave function Ψ_T analytically. However, the Monte Carlo method provides an opportunity to evaluate them numerically. The variational Monte Carlo (VMC) is such a method which is based on a combination of the variational principle and the Monte Carlo evaluation of integrals.

The straightforward Monte Carlo sampling to integrate $E[\Psi_T]$ is inefficient. A better choice is to rewrite Eq. 2.7 as

$$E[\Psi_T] = \frac{\langle \Psi_T^* | H | \Psi_T \rangle}{\langle \Psi_T^* | \Psi_T \rangle} = \frac{\int \Psi_T \hat{H} \Psi_T d\mathbf{R}}{\int |\Psi_T|^2 d\mathbf{R}} = \frac{\int |\Psi_T|^2 (\Psi_T^{-1} \hat{H} \Psi_T) d\mathbf{R}}{\int |\Psi_T|^2 d\mathbf{R}} \quad 2.8$$

If we set up the normalized probability density function of the electrons as

$$P(\mathbf{R}) = \frac{|\Psi_T|^2}{\int |\Psi_T|^2 d\mathbf{R}} \quad 2.9$$

and define the “local energy” E_L as

$$E_L = \Psi_T^{-1} \hat{H} \Psi_T \quad 2.10$$

Eq. 2.8 can be rewrite as

$$E[\Psi_T] = \int P(\mathbf{R}) E_L d\mathbf{R} \quad 2.11$$

The rewriting Eq.2.7 to Eq.2.11 has two advantages. First, Eq.2.11 is now in the form of a weighted average rather than an operator expectation value in Eq. 2.7. The weight here is the normalized probability density function of the electrons $P(\mathbf{R})$. Second, the local energy, E_L , has the property that it is a constant for an eigenfunction of H , since $H\Phi_k = E_k\Phi_k$, we have $E_L[\Phi_k] = E_k$. This property is significant because this means that Eq.2.11 can give E_k with zero variance. In practice, the trial wave function is rarely an eigenfunction. However, a less variance local energy E_L can be obtained with a more accurate trial wave function Ψ_T .

Now we can use the Metropolis algorithm to sample a set of points $\{R_m: m=1:M\}$ from the probability density function of the electrons $P(R)$. At each of these points, the local energy E_L is evaluated. The integral of Eq.2.11 can be replaced by using a summation

$$E[\Psi_T] = \int P(\mathbf{R}) E_L d\mathbf{R} \approx \frac{1}{M} \sum_{m=1}^M E_L(\mathbf{R}_m) \quad 2.12$$

Assuming uncorrelated sampling, the variance of the mean value is given by

$$\sigma^2(E[\Psi_T]) = \frac{\langle E_L^2 \rangle_{\Psi_T^2} - \langle E_L \rangle_{\Psi_T^2}^2}{M - 1} \quad 2.13$$

The whole process of VMC calculation is shown in Figure. 2.1. First, we generate a set of random walkers. A trial step from the point R to R' in the $3N$ dimensional phase space of electron positions is made by moving one or more electrons. Eq. 2.14 then gives the probability of accepting the trial move

$$A = \text{MIN} \left(\frac{\Psi^2(\mathbf{R}')}{\Psi^2(\mathbf{R})}, 1 \right) \quad 2.14$$

The closer Ψ_T is to the true ground state wave function the more accurate our ground state estimate will be. However, it is always difficult to find an accurate enough trial wave function to recover more than 80-90% of the correlation energy using the VMC method³⁷. The main use of the VMC calculation is to provide an initial guess to a more accurate method, DMC method, which will be discussed in the next section.

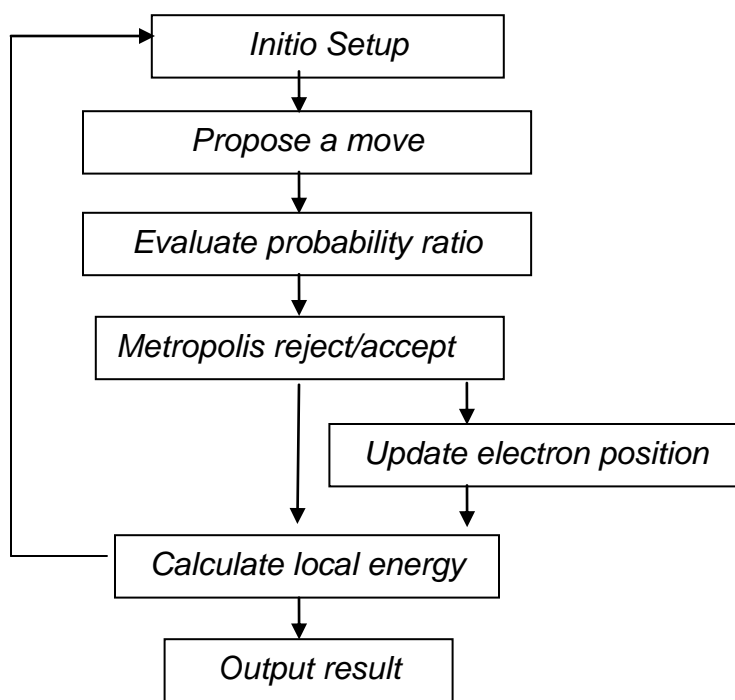


Figure 2.1 The process of the Variational Monte Carlo (VMC) calculation

2.4 DIFFUSION MONTE CARLO

2.4.1 Introduction

The Diffusion Monte Carlo (DMC) method is a stochastic approach to obtain the ground state solution through a random walk simulation of the imaginary-time Schrödinger equation^{29,36}. The name of this method comes from its underlying connection to a diffusion problem. Consider the imaginary-time Schrödinger equation

$$\frac{\partial}{\partial \tau} \Psi(\bar{R}, \tau) = \sum_i^N \frac{1}{2m_i} \nabla_i^2 \Psi(\bar{R}, \tau) + [E_T - V(\bar{R})] \Psi(\bar{R}, \tau) \quad 2.15$$

where $\bar{R} \equiv \{\bar{r}_1, \bar{r}_2, \dots, \bar{r}_N\}$ represents a spatial configuration of the system, τ is the imaginary time, E_T is an arbitrary energy shift, and $\hbar = 1$ in atomic units. We can see that without the second term on the right hand side, Eq. 2.15 is the usual multi-dimensional diffusion equation, and the wave function $\Psi(\bar{R}, \tau)$ can be interpreted as a probability density in a diffusion progress where diffusion constants are defined as $D_i = 1/2m_i (i = 1 \dots N)$. Alternatively, ignoring the first term on the right hand side of Eq. 2.15 and retaining the second term results in a first-order rate equation whose rate constant is $(E_T - V)$. Both diffusion and rate processes can be simulated separately by the Monte Carlo methods. It is therefore reasonable to expect that the entire equation could be simulated by a combined stochastic process consisting of diffusion plus branching. However, it is not advisable to solve differential equations directly using the Monte Carlo methods. Rather, the Monte Carlo methods are good at creating a Markov chain of states and estimating integrals. In connection with these capabilities, it is necessary to recast Eq. 2.15 into an iterative integral equation.

2.4.2 The Green's Function Propagator

Using the Dirac bracket notation, the formal solution of Eq. 2.15 can be written as

$$|\Psi(\tau + \delta\tau)\rangle = e^{-(\hat{H}-E_T)\delta\tau} |\Psi(\tau)\rangle \quad 2.16$$

where \hat{H} is the system Hamiltonian and E_T is an energy shift. By inserting a complete set of position states between the exponential operator and $|\Psi(\tau)\rangle$ in Eq.2.16, and multiplying on the left by $\langle \bar{R}' |$ we get

$$\Psi(\bar{R}', \tau + \delta\tau) = \int \langle \bar{R}' | e^{-(\hat{H}-E_T)\delta\tau} | \bar{R} \rangle \Psi(\bar{R}, \tau) d\bar{R} \quad 2.17$$

Define the *Green's function* to be

$$G(\bar{R}', \tau + \delta\tau; \bar{R}, \tau) \equiv \langle \bar{R}' | e^{-(\hat{H}-E_T)\delta\tau} | \bar{R} \rangle \quad 2.18$$

The expression of Eq. 2.18 shows that the Green's function depends only on the time difference $\delta\tau$. Hence we can rewrite Eq. 2.17 as

$$\Psi(\bar{R}', \tau + \delta\tau) = \int G(\bar{R}', \bar{R}; \delta\tau) \Psi(\bar{R}, \tau) d\bar{R} \quad 2.19$$

In the Monte Carlo applications, $G(\bar{R}', \bar{R}; \delta\tau)$ is positive everywhere and normalizable. It may be interpreted as a transition probability. Then Eq. 2.19 may be simulated by a random walk process in which $G(\bar{R}', \bar{R}; \delta\tau)$ is the probability of moving from \bar{R} to \bar{R}' in an imaginary time interval $\delta\tau$. Since $G(\bar{R}', \bar{R}; \delta\tau)$ is independent of time and history, the random walk constitutes a Markov chain, and an equilibrium distribution of walkers will be achieved after a sufficient long time.

To illustrate the convergence of this process we can expand $G(\bar{R}', \bar{R}; \delta\tau)$ in the eigenfunctions of \hat{H} by inserting two complete sets of states into Eq.2.18,

$$G(\bar{R}', \bar{R}; \delta\tau) = \sum_{i=0}^{\infty} e^{-(E_i - E_T)\delta\tau} \Phi_i(\bar{R}') \Phi_i(\bar{R}) \quad 2.20$$

and substitute this into Eq. 2.19 while also using $\Psi(\bar{R}, 0) = \sum_k C_k \Phi_k(\bar{R})$ to obtain the first iteration,

$$\begin{aligned} \Psi(\bar{R}', \delta\tau) &= \int \sum_{i=0}^{\infty} e^{-(E_i - E_T)\delta\tau} \Phi_i(\bar{R}') \Phi_i(\bar{R}) \sum_{k=0}^{\infty} C_k \Phi_k(\bar{R}) d\bar{R} \\ &= \sum_{k=0}^{\infty} C_k \Phi_k(\bar{R}') e^{-(E_k - E_T)\delta\tau} \end{aligned} \quad 2.21$$

After n iterations we have

$$\Psi(\bar{R}', n\delta\tau) = \sum_{k=0}^{\infty} C_k \Phi_k(\bar{R}') e^{-(E_k - E_T)n\delta\tau} \quad 2.22$$

At large n , the lowest energy component with a non-zero coefficient will dominate the sum, which generally will be the ground state, unless $\Psi(\bar{R}, 0)$ is specially chosen so that it is orthogonal to the ground state. As a simulation to this iterative process, the random walk will correspondingly achieve an equilibrium state at the same time, in which the population density of walkers represents the ground state wave function.

2.4.3 The Short Time Approximation

So far we see that the imaginary-time Schrödinger equation Eq. 2.15 can be solved by a random walk simulation and the ground state wave function may be obtained in the form of probability density of walkers after a sufficient long walking. However, there is an unsolved difficulty for implementing this approach in practice, i.e., the exact Green's function is generally not known. Fortunately, an analytic (though approximate) expression for the Green's function is available

for the random walk simulation, if a very short imaginary-time interval between successive iterations of Eq. 2.19 is assumed. That is,

$$G = e^{-(\hat{T} + \hat{V} - E_T)\tau} \approx e^{-\hat{T}\tau} e^{-(\hat{V} - E_T)\tau} \equiv G_{diff} G_B \quad (\tau \rightarrow 0) \quad 2.23$$

We can identify G_{diff} as the Green's function of the classical diffusion equation and G_B as the Green's function of the rate equation, i.e.,

$$G_{diff}(\vec{R}', \vec{R}; \tau) = \prod_{i=1}^N (4\pi D_i \tau)^{-3/2} e^{-(\vec{r}_i' - \vec{r}_i)^2 / 4D_i \tau} \quad 2.24$$

$$G_B(\vec{R}', \vec{R}; \tau) = e^{-\frac{1}{2}[V(\vec{R}') + V(\vec{R})] - E_T \tau} \quad 2.25$$

The error of this approximation comes from the fact that \hat{T} and \hat{V} do not commute. The first correction term is of the form

$$G - G_{diff} G_B = \frac{1}{2} [\hat{V}, \hat{T}] \tau^2 + O(\tau^3) \quad 2.26$$

Therefore we can rewrite Eq. 2.19 in terms of the diffusion Green's function propagator and the branching Green's function propagator, without significant errors as long as τ is very small,

$$\Psi(\vec{R}', \tau + \delta\tau) = \int G_{diff}(\vec{R}', \vec{R}; \delta\tau) G_B(\vec{R}', \vec{R}; \delta\tau) \Psi(\vec{R}, \tau) d\vec{R} \quad 2.27$$

2.4.4 The Simple Sampling

The diffusion part in the Monte Carlo iteration of Eq. 2.27 can be simply simulated by random Gaussian displacement of the Cartesian coordinates

$$\vec{r}_i(\tau + \delta\tau) = \vec{r}_i(\tau) + \vec{g}_i \sqrt{2D_i \delta\tau} \quad 2.28$$

where the index i run over all the quantum particles being considered and \bar{g} is a vector of random number chosen from a Gaussian distribution with unit variance. The branching part can be simulated by the creation or destruction of walkers with probability G_B . A discrete method to implement the branching selection is to calculate an integer B , which equals the integral part of $(G_B + \eta)$, where η is a random number uniformly distributed over $[0, 1]$. If B is zero, the walker is eliminated; otherwise the population is increased to give B copies of the walker.

Alternatively, G_B can be taken into account by assigning a weight to each walker. In this situation the random walk is carried out without branching, leaving the population constant. To illustrate this approach, suppose we start the random walk simulation of Eq. 2.27 with an initial distribution sampled from $\Psi(\bar{R}_0, 0)$ and iterate the equation n times, visiting the intermediate states $\bar{R}_1, \bar{R}_2, \dots, \bar{R}_{n-1}$. The final distribution $\Psi(\bar{R}_n, n\delta\tau)$ will be given by the integral over the intermediate states,

$$\begin{aligned} \Psi(\bar{R}_n, \tau + n\delta\tau) = & \int G_{diff}(\bar{R}_n, \bar{R}_{n-1}; \delta\tau) G_B(\bar{R}_n, \bar{R}_{n-1}; \delta\tau) d\bar{R}_{n-1} \\ & \times \int G_{diff}(\bar{R}_{n-1}, \bar{R}_{n-2}; \delta\tau) G_B(\bar{R}_{n-1}, \bar{R}_{n-2}; \delta\tau) d\bar{R}_{n-2} \\ & \vdots \\ & \times \int G_{diff}(\bar{R}_1, \bar{R}_0; \delta\tau) G_B(\bar{R}_1, \bar{R}_0; \delta\tau) \Psi(\bar{R}_0, 0) d\bar{R}_0 \end{aligned} \quad 2.29$$

If we define the branching weight $w(\bar{R}_i) \equiv G_B(\bar{R}_i, \bar{R}_{i-1}; \delta\tau)$, Eq. 2.29 can be rewritten as

$$\begin{aligned} \Psi(\bar{R}_n, \tau + n\delta\tau) = & \int G_{diff}(\bar{R}_n, \bar{R}_{n-1}; \delta\tau) G_{diff}(\bar{R}_{n-1}, \bar{R}_{n-2}; \delta\tau) \cdots G_{diff}(\bar{R}_1, \bar{R}_0; \delta\tau) \\ & \times \left\{ \prod_{i=1}^n w(\bar{R}_i) \right\} \Psi(\bar{R}_0, 0) d\bar{R}_{n-1} d\bar{R}_{n-2} \cdots d\bar{R}_0 \end{aligned} \quad 2.30$$

Therefore the proper weight to be associated with each walker is the cumulative product of the branching weights. For a walker ending at \bar{R}_n , the cumulative weight can be defined as $W(\bar{R}_n)$,

$$W(\bar{R}_n) = \prod_i^n w(\bar{R}_i) \quad 2.31$$

The cumulative weights should be always counted in when statistical quantities, such as expectation values and variances, are estimated.

The advantage of this continuous weighting approach is that the population of the walkers remains constant rather than fluctuating around its initial size. As a result, the statistical variance is reduced. Also, computational benefit is gained by the elimination of the need to dynamically adjust storage requirement. However, there is a problem with it. At long time one can see that the cumulative weight of a walker will either become very large (if $w(\bar{R})$ is on average greater than one) or vanish (if $w(\bar{R})$ is smaller than one on average). In an ensemble both behaviors may be present. Thus some walkers with nearly zero weight are kept together with others with relatively large weight. After a sufficient large number of iterations the energy estimate will be dominated by a single walker, while a growing population of walkers will effectively contribute nothing to the average. In this case, the sampling of the wave function will be poor and statistical errors will be large correspondingly. This problem can be overcome by a suitable compromise between the branching and the weighting approaches. Any walker whose weight falls below a certain critical threshold is eliminated. When this happens, the walker with the largest weight is split into two of equal weight, one of which occupies the storage location formerly associated with the destroyed walker. This procedure ensures a fixed number of walkers and a reasonable range of weight, at the price of a small error introduced by incorrect boundary conditions. But as long as the lower limit of weight at which the “repacking” is carried out is small enough, the error introduced is negligible. The use of importance sampling will also decrease the error.

2.4.5 Importance Sampling

There are often significant statistical errors associated with the simple random walk simulation described in the previous section. The error can be reduced partly by the proper choice of the simulation parameters such as the time step and the population size. In addition, it is usually possible to improve the accuracy of the simulation by the Monte Carlo technique of importance sampling^{31,38}. In this procedure, one constructs an analytical trial function, Φ_T , based on any available knowledge of the true ground state wave function Φ_0 . The trial function is then used to bias the random walk to produce the distribution $f(\bar{R}, \tau) \equiv \Psi(\bar{R}, \tau)\Phi_T(\bar{R}, \tau)$ rather than $\Psi(\bar{R}, \tau)$. Accordingly, the diffusion process is modified by a drift due to a vector field $\vec{F}_i(\bar{R}) \equiv \nabla_i \ln|\Phi_T|^2 = 2\nabla_i \Phi_T / \Phi_T$, usually referred as the ‘quantum force’, which directs the random walkers away from regions where the trial wave function is small and therefore enhance the sampling efficiency. The diffusion Green’s function is modified as

$$\tilde{G}_{diff}(\bar{R}', \bar{R}; \delta\tau) = \prod_{i=1}^N (4\pi D_i \delta\tau)^{-3/2} e^{-(\bar{r}_i' - \bar{r}_i - D_i \delta\tau \vec{F}_i(\bar{R}))^2 / 4D_i \delta\tau} \quad 2.32$$

And Eq. 2.28 changes to

$$\bar{r}_i(\tau + \delta\tau) = \bar{r}_i(\tau) + \bar{g} \sqrt{2D_i \delta\tau} + D_i \delta\tau \vec{F}_i(\bar{R}) \quad 2.33$$

The potential term in the branching weight is now replaced by the local energy term $E_L(\bar{R}) \equiv \hat{H}\Phi_T / \Phi_T$,

$$\tilde{w}(\bar{R}') \equiv \tilde{G}_B(\bar{R}', \bar{R}; \delta\tau) = e^{-\frac{1}{2}[E_L(\bar{R}') + E_L(\bar{R}) - E_T] \delta\tau} \quad 2.34$$

The local energy term contains both kinetic and potential contributions and is much smoother than the potential term alone. If by chance we choose the exact wave function as the

trial function, the branching weight will simply be a constant and the fluctuation of the population size (total weight) will be completely eliminated.

It is necessary to impose “detailed balance” in order to guarantee equilibrium, since now $\tilde{G}_{diff}(\bar{R}', \bar{R}; \delta\tau) \neq \tilde{G}_{diff}(\bar{R}, \bar{R}'; \delta\tau)$. Detailed balance is achieved by accepting the move of the walker from \bar{R} to \bar{R}' with the Metropolis probability

$$A(\bar{R}', \bar{R}; \delta\tau) \equiv \min(1, q(\bar{R}', \bar{R}; \delta\tau)) \quad 2.35$$

where

$$q((\bar{R}', \bar{R}; \delta\tau)) \equiv \frac{|\Phi_T(\bar{R}')|^2 \tilde{G}_{diff}(\bar{R}, \bar{R}'; \delta\tau)}{|\Phi_T(\bar{R})|^2 \tilde{G}_{diff}(\bar{R}', \bar{R}; \delta\tau)} \quad 2.36$$

This step insures that the distribution converges to $\Phi_T \Phi_0$ as $\delta\tau \rightarrow 0$.

2.4.6 Fixed Node Approximation

A fundamental requirement when solving the electronic Schrödinger equation is that an electronic wave function is antisymmetric on interexchange of any two electrons. It is Pauli Exclusion Principle for Fermion system as

$$\Phi_e(\cdots x_i \cdots x_j) = -\Phi_e(\cdots x_j \cdots x_i) \quad 2.37$$

Thus there are bound to be regions where the wave function is positive and others where it is negative. The central difficulty in the DMC simulation of Fermions is that the wave function is represented by a density of random walkers, which should be positive everywhere. This constraint is acceptable for describing Bosonic wave -functions, but leads to problems in Fermion wave functions, which have both positive and negative regions, and node surface

dividing these regions. To simulate such systems we must find a method of maintaining a positive density of walkers everywhere, while still enforcing the antisymmetry condition.

There are several methods that impose the antisymmetry in the DMC simulation^{29,30,39,40}. The fixed-node method^{29,30} is the most popular one. Recalling Eq. 2.15 with the importance sampling technique, the imaginary-time Schrödinger equation can be written as

$$-\frac{\partial f(\vec{R}, \tau)}{\partial \tau} = -D\nabla^2 f + D\nabla \cdot [fF_Q(\vec{R})] + [E_L(\vec{R}) - E_T]f \quad 2.38$$

where the density function $f(\vec{R}, \tau) \equiv \Psi(\vec{R}, \tau)\Phi_T(\vec{R}, \tau)$ must be non-negative. This can be guaranteed if we constrain $\Psi(\vec{R}, \tau)$ to have the same sign as the trial wave function, $\Phi_T(\vec{R}, \tau)$, everywhere in phase space. The best that we can then do is to find the lowest energy wave function with the same nodal surface as the trial wave function. This idea of constraining the nodal surface of Ψ is the basis of the fixed-node approximation, and is very easy to implement within DMC. Within the short time approximation, the fixed-node approximation is implemented by rejecting walker trial moves that try to cross into a region of Φ_T with opposite sign³⁸.

The fixed-node solution of the electronic Schrödinger equation can be viewed as occurring separately within each nodal pocket. It was proved by Ceperley⁴¹ that for the ground state of any N electrons system, all these nodal pockets are equivalent. The separate solutions of the fixed-node Schrödinger equation within each nodal pocket therefore all give the same energy. Therefore, we only need to sample only one of its pockets.

The DMC energy is always greater than the exact ground unless the trial node surface is exact. However, since most trial wave functions are obtained from Hartree-Fock or DFT calculations, and since such calculations usually give physically reasonable results for Coulomb

systems, it is hoped that the imposed nodal surface is not too far from the true one, and hence that the fixed-node energy is close to the true Fermion ground state energy.

2.5 TRIAL WAVE FUNCTION

Before the QMC simulation is able to be implemented, we must first choose a suitable trial wave function for the system to be studied. The choice of the trial wave function is important for both VMC and DMC calculation. In VMC, it determines the ultimate accuracy because all averages are evaluated with respect to the trial wave function. In fixed-node DMC, it not only determines the quality of the nodes, but also affects the variance of the calculation.

Unlike conventional electronic structure methods, in which the wave function is restricted to be a Slater determinant (or linear combination of determinants) of one-electron orbitals, QMC methods have an ability to use arbitrary wave function forms. Given this flexibility, it is important to recall properties a trial wave function ideally should possess, such as the cusp condition⁴².

Several types of trial wave function have been used for the many-electrons problem, among which the Slater-Jastrow⁴³ function is one of the most popular wave functions used in DMC. This function is expressed as

$$\Psi_T(R) = \Psi_D(R)e^{J(R)} \quad 2.39$$

where $\Psi_D(R)$ is the Slater determinant, which incorporates the antisymmetric requirement of a Fermion wave function, and $e^{J(R)}$ is the Jastrow function, which represents the electron correlation. $\Psi_D(R)$ comprises molecular orbitals (or Bloch functions expanded in plane

waves for solids) as its matrix elements. Linear combinations of Slater determinants are also sometimes used. The Jastrow factor in this paper is the sum of homogeneous, isotropic electron-electron terms u , isotropic electron-nucleus terms χ centered on the nuclei, isotropic electron-electron-nucleus terms f , also centered on the nuclei⁴⁴. The form is

$$J(r_i, r_l) = \sum_{i=1}^{N-1} \sum_{j=i+1}^N u(r_{ij}) + \sum_{I=1}^M \sum_{i=1}^N \chi_I(r_{iI}) + \sum_{I=1}^M \sum_{i=1}^{N-1} \sum_{j=i+1}^N f_I(r_{iI} + r_{jI} + r_{ij}) \quad 2.40$$

where N is the number of electrons, M is the number of ions, $r_{ij} = r_i - r_j$, $r_{iI} = r_i - r_I$, r_i is the position of electron i and r_I is the position of nucleus I . Note that u , χ , and f terms may also depend on the spins of electrons i and j .

The u term consists of a complete power expansion in r_{ij} up to order $r_{ij}^{C+N_u}$ which satisfies the Kato cusp conditions at $r_{ij} = 0$, goes to zero at the cutoff length, $r_{ij} = L_u$, and has $C - 1$ continuous derivatives at L_u :

$$u(r_{ij}) = (r_{ij} - L_u)^C \times \Theta(L_u - r_{ij}) \times (\alpha_0 + [\frac{\Gamma_{ij}}{(-L_u)^C} + \frac{\alpha_0 C}{L_u}]r_{ij} + \sum_{l=2}^{N_u} \alpha_l r_{ij}^l) \quad 2.41$$

where Θ is the Heaviside function and $\Gamma_{ij} = 1/2$ if electrons i and j have opposite spins and $\Gamma_{ij} = 1/4$ if they have the same spin. In this expression C determines the behavior at the cutoff length. If $C = 2$, the gradient of u is continuous but the second derivative and hence the local energy is discontinuous, and if $C = 3$ then both the gradient of u and the local energy are continuous.

The form of χ is

$$\chi(r_{iI}) = (r_{iI} - L_{\chi I})^C \times \Theta(L_{\chi I} - r_{iI}) \times (\beta_{0I} + [\frac{-Z_i}{(-L_{\chi I})^C} + \frac{\beta_{0I} C}{L_{\chi I}}]r_{iI} + \sum_{m=2}^{N_\chi} \beta_{mI} r_{iI}^m) \quad 2.42$$

It may be assumed that $\beta_{mI} = \beta_{mJ}$ where I and J are equivalent ions. The term involving the ionic charge Z_I enforces the electron-nucleus cusp condition.

The expression for f is the most general expansion of a function of r_{ij} , r_{iI} and r_{jI} that does not interfere with the Kato cusp conditions and goes smoothly to zero when either r_{iI} or r_{jI} reach cutoff lengths:

$$f_I(r_{iI}, r_{jI}, r_{ij}) = (r_{iI} - L_{fI})^C (r_{jI} - L_{fI})^C \Theta(L_{fI} - r_{iI}) \Theta(L_{fI} - r_{jI}) \sum_{l=0}^{N_{fI}^{eN}} \sum_{m=0}^{N_{fI}^{eN}} \sum_{n=0}^{N_{fI}^{ee}} \gamma_{lmnl} r_{iI}^l r_{jI}^m r_{ij}^n \quad 2.43$$

Various restrictions are placed on γ_{lmnl} . To ensure the Jastrow factor is symmetric under electron exchanges it is demanded that $\gamma_{lmnl} = \gamma_{mnlm} \forall I, m, l, n$. If ions I and J are equivalent then it is demanded that $\gamma_{lmnl} = \gamma_{mnlm}^J$.

3.0 THE QMC STUDY OF THE BE ATOM

3.1 INTRODUCTION

With the development of the *ab initio* methods, one can determine the electronic structure of systems with many electrons only by invoking a number of approximations. For systems like beryllium with only a few electrons, high-level "complete" nonrelativistic calculations are within reach, and these benchmark calculations have become important sources of information concerning the accuracy of the various algorithms, approximations, and basis sets.

The HF description of the ground state of the Be atom (1S) gives the electronic configuration $1s^22s^2$. However, because the $1s^22p^2$ electronic configuration is almost degenerate with the previous one, Beryllium is also challenging for the *ab initio* techniques.

3.2 COMPUTATIONAL DETAILS

We did all-electron calculations of the ground-state energy of the Be atom using the variational and diffusion quantum Monte Carlo (VMC and DMC) methods. Accurate approximations to the many-electron wave function are required as inputs for the VMC and DMC methods⁴⁵. The quality of these "trial" wave functions determines both the statistical efficiency of the methods and the final accuracy that can be obtained.

Several different forms of trial wave function were used here: (a) RHF orbitals with optimized Jastrow function, (b) UHF orbitals with optimized Jastrow function, (c) Brueckner Doubles (BD)^{46,47} orbitals with optimized Jastrow function, and (d) CASSCF orbitals with optimized Jastrow function.

The basic form of the wave functions consists of a product of Slater determinants for spin-up and spin-down electrons containing the orbitals, such as RHF, UHF, and BD orbitals, multiplied by a positive Jastrow correlation factor. We have also carried out some tests using multideterminant wave functions like CASSCF orbitals in the study.

The RHF, UHF, BD, and CASSCF orbitals forming the Slater determinants were obtained from the calculations using Gaussian03 code⁴⁸. 6-311G(d) basis sets were used for all calculation.

All the variational and diffusion quantum Monte Carlo (VMC and DMC) calculations were performed using the CASINO code⁴⁹. In the VMC calculation, the number of equilibration moves at the start of the calculation is all set to be 5000, which are substantially large enough in order to ensure that all of the transient effects due to the initial distribution die away. The total VMC steps are set to be 40000. All of the DMC calculations were performed with a target population of 1200 configurations (walkers). The parameters in the Jastrow functions were obtained by minimizing the variance of the local energy^{50,51}. All of the energies were extrapolated to zero time step.

3.3 RESULTS

In Table 3.1 we present values for the total nonrelativistic energies of the Be atom, calculated using a number of different electronic-structure methods. For comparison, We give results obtained using RHF, UHF, BD, and Cas(2,4) methods with 6-311G(d) basis sets, as well as the VMC and DMC methods with the RHF, UHF, BD, and Cas(2,4) trail wave functions, respectively.

Table 3.1 Total energy of the Be atom calculated with different *ab initio* methods, and the experimental result.

Method	Energy (a.u.)
RHF/6-311G(d)	-14.5718739
UHF/6-311G(d)	-14.5722037
BD/6-311G(d)	-14.6172223
Cas(2,4)/6-311G(d)	-14.6118491
HF ⁵²	-14.573023
VMC-RHF (no Jastrow function)	-14.567(7)
VMC-UHF (no Jastrow function)	-14.575(4)
VMC-BD (no Jastrow function)	-14.575(4)
VMC-Cas(2.4) (no Jastrow function)	-14.621(7)
VMC-RHF (with Jastrow function)	-14.6296(7)
VMC-UHF (with Jastrow function)	-14.6244(9)
VMC-BD (with Jastrow function)	-14.6266(9)
VMC-Cas(2.4) (with Jastrow function)	-14.660(1)
DMC-RHF	-14.6577(7)
DMC-UHF	-14.6560(5)
DMC-BD	-14.6581(4)
DMC-CAS(2,4)	-14.6663(3)

CCSD(T)/cc-pVTZ ⁵³	-14.623790
FCI/cc-pVTZ ⁵³	-14.623810
Explicitly correlated Gaussians ⁵⁴	-14.667355(1)
Experiment, minus relativistic corrections ⁵³	-14.66736(1)
Experiment ⁵²	-14.6693324(1)

We performed both VMC(no Jastrow function) and VMC (with Jastrow function) calculations. The results of VMC-RHF(no Jastrow function), VMC-UHF(no Jastrow function), and VMC-Cas(2,4) (no Jastrow function) agree with that of RHF, UHF, and Cas(2.3) method, since the VMC energy is calculated as the expectation value of the Hamiltonian operator with respect to a trial wave function. However, the result of VMC-BD(no Jastrow function) does not match that of the BD method, but agrees with that of the HF method. It is not surprised because in the absence of the perturbation, the single Brueckner determinant, which is used in the VMC calculation, is identical with the Hartree-Fock single determinant⁴⁷. With the optimized Jastrow function, all of the VMC results with different trial wave functions are improved. Our VMC energies with RHF+Jastrow, UHF+Jastrow, BD+Jastrow, and Cas(2,4)+Jastrow are -14.6296(7), -14.6244(9), -14.6266(9), and -14.660(1), respectively. These values are lower than the energies from CCSD(T)/cc-pVTZ and FCI/cc-pVTZ calculations. However, the accuracy of a VMC simulation was entirely limited by the quality of the trial wave function. While they are lower than their respective RHF, UHF, BD, and CASSCF equivalents, they are still significantly higher than our DMC energies and the “exact” result.

In DMC calculations, all of the energies were extrapolated to zero time. We used a range of small time steps and performed linear extrapolations of the energies to zero time step. The DMC energies with all of the four different trial wave functions, RHF, UHF, BD, and Cas(2,4), are at most 12 mhartree, above the exact result of -14.667355(1). The DMC energy with Cas(2,4)

nodal surface performs best, which is only about 1 mhartree above the exact one. Therefore, all of the four trial wave functions, RHF, UHF, BD, and Cas(2,4), can provide agreeable nodal surfaces for the fixed-node DMC calculation of the Be atom. The DMC-Cas(2,4) can give the best result in all of the four choices of the trial wave functions.

Multi-determinant wave functions, such as Cas(2,4), performs better than single-determinant wave functions. However, the DMC energy with Cas(2,4) and 6-311G(d) basis set is still 1 mhartree higher than the exact one. To obtain more improvement, more active spaces Cas(2, 10) in which 2s2p3s3d orbitals are included, are applied as trial functions in the DMC calculations. Two different basis sets, CVB2⁵⁵ and ADF-QZ4Pae-f⁵⁶ were used to compare to 6-31G(d) basis set to see which one can provide a better nodal surface. Table 3.2 shows the DMC energy of the Be atom with different Cas(2,4) and Cas(2,10) trial functions with different basis sets. It can be seen that with the same active space Cas(2,4) including 2s2p, the DMC energy with CVB1basis set is about 0.0009 hartree lower than the one with 6-31G(d) basis sets. With Cas(2,10) (2s2p3s3d) trial functions, the DMC energy with CVB2 basis set performs better than the one with ADF basis set for about 0.0004 hartree. The trial function Cas(2,10) with CVB2 basis set gives the best nodal surface and the DMC energy is very close to the exact result of -14.667355(1), and only about 0.00006 hartree higher.

Table 3.2 DMC energy of the Be atom calculated with different Cas trial functions.

Method	Energy (a.u.)
DMC-CAS(2,4)/6-31G(d)	-14.6663(3)
DMC-CAS(2,4)/CVB1	-14.66727(1) ⁵⁷
DMC-CAS(2,10)/CVB2	-14.66729(3)
DMC-CAS(2,10)/ADF	-14.66687(5)
Explicitly correlated Gaussians ⁵⁴	-14.667355(1)

4.0 THE QMC STUDY OF WATER DIMER

4.1 INTRODUCTION

Water is the main agent of all aqueous phenomena. It is also an important component of the vast majority of all chemical and biological processes. The description of the structure and energetics of assemblies of water molecules has been the subject of many experimental and theoretical studies, as this knowledge is vital to the understanding of water in all its physical states.

The characteristic physical and chemical properties of water are mostly from its hydrogen bonds. In spite of the apparent simplicity of hydrogen bonding, understanding hydrogen bonding remains a challenge, due in part to the relative weakness of the interaction.

The water dimer has been the subject of many electronic structure studies⁵⁸⁻⁶¹, since it represents the prototype of all hydrogen-bonded systems. Despite its apparent simplicity, accurate theoretical descriptions of the water dimer have typically required the use of very large basis sets in combination with sophisticated wave function techniques, such as the configuration interaction (CI) method and the coupled cluster (CC) method. These methods can perform high accuracy. However they are slowly convergent and scale badly with system size. They also suffer from basis set superposition and basis set incompleteness errors. Density functional theory (DFT) is a computationally economical choice. Unfortunately, DFT meet challenges to treat dispersion interactions accurately, which is important for studying hydrogen bond systems.

The Quantum Monte Carlo (QMC) method is another promising choice in situations where high accuracy is required. We performed all-electron variational quantum Monte Carlo (VMC) and diffusion quantum Monte Carlo (DMC) calculations of the total energy of the water monomer and dimer. The equilibrium dissociation energy D_e of the water dimer was deduced by subtracting the sum of the energies of two monomers from the water dimer energy.

The accuracy of the VMC method depends crucially on the trial wave functions. The fixed-node DMC energy also depends on the quality of the nodal surface of the trial wave functions. Fortunately, the error induced by the fixed-node approximation should largely cancel when energy differences, such as equilibrium dissociation energies, are calculated⁶². This cancellation was tested to be almost perfect for weakly bound systems⁶³. The trial wave function of the Slater-Jastrow form, which consists of a product of Slater determinants and a positive Jastrow function, was used in the VMC and DMC calculations. The Slater determinants were obtained from Hartree-Fock (HF) method with aug-cc-pVDZ basis sets. The basis set used for the DMC calculation can be smaller than that for other highly accurate methods, such as MP2, or CCSD(T), since the energies obtained in the DMC method depend less strongly on the quality of the basis set⁶². The parameters in the Jastrow functions were obtained by minimizing the variance of the local energy^{50,64}.

4.2 COMPUTATIONAL DETAILS

All the variational and diffusion quantum Monte Carlo (VMC and DMC) calculations were performed using the CASINO code⁶⁵. In the VMC calculation, the number of equilibration moves at the start of the calculation is all set to be 5000, which are substantially large enough in

order to ensure that all of the transient effects due to the initial distribution die away. The total VMC steps are set to be 40000. All of the DMC calculations were performed with a target population of 1600 configurations (walkers). Time-step errors have been carefully checked. All of the energies were extrapolated to zero time step.

The calculations for the water monomer were carried out at the experimental equilibrium geometry⁶⁶ $r_{\text{OH}}=r'_{\text{OH}} = 0.9572 \text{ \AA}$ and $\angle_{\text{HOH}} = 104.52^\circ$. This geometry has been used in previous calculations on the water monomer^{61,62,67}.

For the water dimer we chose the geometry optimized from the MP2/aug-cc-pv5z calculations. The optimized water dimer geometry (see Figure.4.1) yields a final equilibrium oxygen-oxygen distance of 2.9098 Å. When the dimer is formed, a slight deformation occurs in each of the monomers. These small changes were neglected, since their effect on the intermolecular binding energy is small⁶¹. The coordinates of water dimer are given in Table 4.1

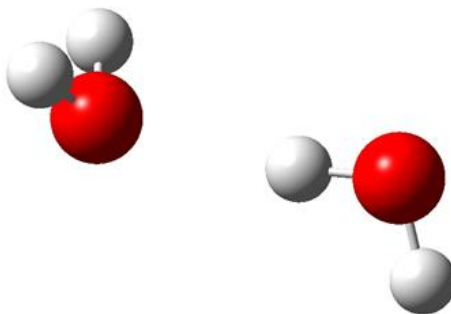


Figure 4.1 The equilibrium structure of the water dimer

Table 4.1 Coordinates of the water dimer in Å

Atom	x	y	z
O	0.00000	0.00000	0.00000
H	-0.31547	-0.49369	-0.75695
H	-0.31547	-0.49369	0.75695
O	2.9098	0.00000	0.00000
H	3.24425	0.89687	0.00000
H	1.957724	0.098906	0.00000

4.3 RESULTS

The results for the total energy of the water monomer from the QMC calculations and from other *ab initio* methods calculations were showed in Table 4.2. The HF/aug-cc-pvdz energy is 0.03 hartree higher than the estimated basis set limit result⁶⁸, which demonstrates the quality of the aug-cc-pvdz basis set is not high enough for HF calculations. Fortunately, the DMC calculations depend less strongly on the quality of the basis set. The accuracy of the VMC simulation was entirely limited by the quality of the trial wave function. While lower than its respective HF equivalents, it was still significantly higher than the DMC energy and the “exact” result. The DMC energy with HF nodes (DMC-HF) is lower than the CCSD(T)/aug-cc-pv5z result, and only 24 mhartree, above the exact result of -76.438 hartree.

Table 4.2 Total energies of the water monomer from various *ab initio* methods

Method	Total energy (a.u.)
HF/aug-cc-pvdz	-76.039
HF limit ⁶⁸	-76.068
CCSD(T)/aug-cc-pv5z ⁶⁹	-76.3703
VMC-HF	-76.331(2)
DMC-HF	-76.4141(5)
“Exact” ⁷⁰	-76.438

Table 4.3 Equilibrium dissociation energies of the water dimer from various *ab initio* methods and the experiment

Method	D_e (kcal/mol)
DMC-HF (this work)	-5.40 ± 0.60
SAPT-5s ⁷¹	-4.86
CCSD(T)-extrapolated ⁷²	-5.02 ± 0.05
DMC (pseudopotential cal.) ⁷³	-5.66 ± 0.20
DMC-HF ⁶²	-5.02 ± 0.18
DMC-B3LYP ⁶²	-5.21 ± 0.18
MP2/CBS limit ⁷⁴	-4.97

Table 4.3 shows the results for the equilibrium dissociation energy of the water dimer. Our DMC energy with HF nodes (DMC-HF) compares very well within the error bars with the CCSD(T) result of Klopper *et al.*⁷² and the MP2/CBS limit result of Xantheas *et al.*⁷⁴ We obtain a lower equilibrium dissociation energy of DMC-HF than that of Benedek *et al.*⁶², although this value is still within the error bars. It should be noted that Benedek *et al.* used the experimentally

determined equilibrium geometry, while we have used a theoretically optimized geometry. They also performed larger DMC steps to obtain a smaller error bar.

5.0 THE QMC STUDY OF WATER CLUSTER ANION

5.1 INTRODUCTION

Water cluster anions provide a model system to unravel how hydrogen-bonded water network deforms to accommodate the excess electron⁹ and help in understanding the free electron hydration at a molecular level. Elucidation of the structures and formation mechanisms of $(\text{H}_2\text{O})_n^-$ clusters is a challenging theoretical problem.^{75,76} In order to quantitatively characterize such clusters using traditional electronic structure methods, it is necessary to employ flexible basis sets with multiple diffuse functions and to include electron correlation effects to high order, e.g. using the CCSD(T) method.^{76,77} Of particular interest are the vertical electron binding energies (EBE), given by the differences in energies of the anionic and neutral clusters at the geometries of the anions. EBEs of $(\text{H}_2\text{O})_n^-$ clusters up through $n = 6$ have been calculated using the CCSD(T) method with large basis sets.^{78,79} In addition, EBEs of $(\text{H}_2\text{O})_n^-$ clusters as large as $(\text{H}_2\text{O})_{30}^-$ have been calculated using the MP2 method but with smaller basis sets.⁸⁰⁻⁸² In some geometrical arrangements there is the complication that the Hartree-Fock method provides a poor description of the anion, and indeed, may even fail to bind the excess electron, which then poses problems for perturbative methods such as MP2.⁸¹

In recent years a new generation of model potential approaches has been developed for treating excess electrons interacting with water clusters.^{76,78,82} These model

potential approaches give EBEs close to the CCSD(T) results for the $n \leq 6$ clusters for which large basis set CCSD(T) calculations have been performed. It is also important to have accurate *ab initio* results for large $(\text{H}_2\text{O})_n^-$ clusters that can serve as benchmarks for testing the computationally faster model potential approaches. In this study, we use the diffusion Monte Carlo (DMC) approach⁸³⁻⁸⁵ to calculate the electron-binding energies of two forms of $(\text{H}_2\text{O})_6^-$. The DMC method is an intriguing alternative to traditional electronic structure approaches for the characterization of $(\text{H}_2\text{O})_n^-$ clusters as its computational effort scales between the third and fourth power with the number of molecules,⁸⁶ and is applicable even in cases where the Hartree-Fock approach does not provide a suitable zeroth-order wave function. The major challenge in using the DMC method to calculate the electron binding energies of $(\text{H}_2\text{O})_n^-$ clusters is the need to run the simulations on the neutral and anionic clusters for a sufficiently large number of moves that the statistical errors in the EBEs are small compared to the EBE values themselves.

5.2 COMPUTATIONAL DETAILS

The two structures of $(\text{H}_2\text{O})_6^-$ considered in this study are shown in Figure 5.1. The geometries employed are the same as those used in Ref. 78. The EBEs of these two species have been previously calculated using flexible basis sets at the Hartree-Fock, MP2, and CCSD(T) levels of theory.^{78,79} Species **A** corresponds to the anion observed experimentally with a measured EBE of 420 meV,⁸⁷ and species **B** has the water molecules arranged as in the Kevan model⁸⁸ of the hydrated electron (e_{aq}^-). **B** is representative of systems for which the Hartree-Fock method drastically underestimates the EBE.

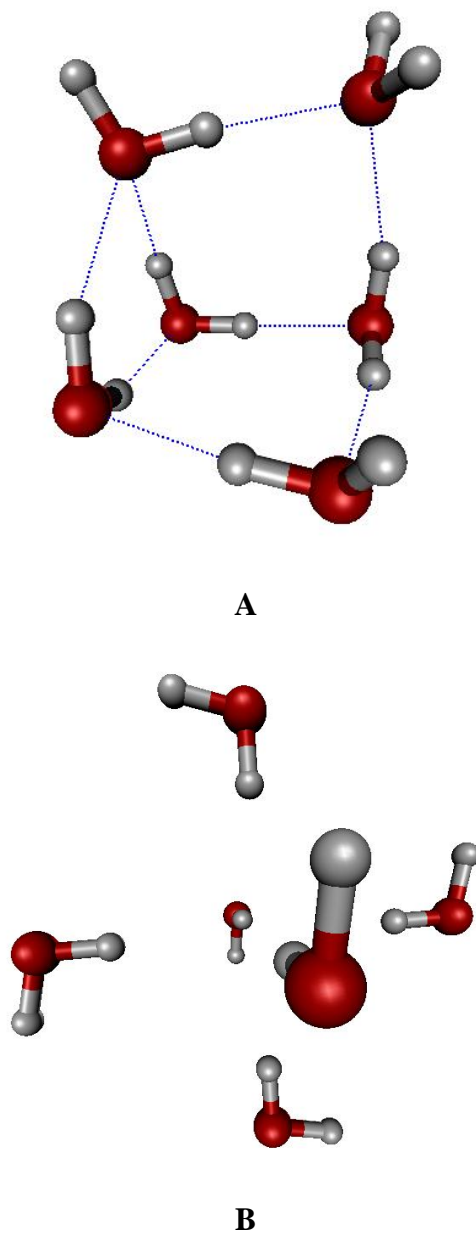


Figure 5.1 Geometrical structures of the A and B forms of $(\text{H}_2\text{O})_6^-$

The DMC calculations were carried out using single-determinantal trial wave functions obtained from Hartree-Fock or Becke3LYP⁸⁹⁻⁹² density functional theory electronic structure calculations, combined with three-term Jastrow factors⁹³ to represent the electron-nuclear and

electron-electron cusps. The parameters in the Jastrow factors were obtained by minimizing the local energy by means of variational Monte Carlo (VMC) calculations.⁹⁴⁻⁹⁶ A Hartree-Fock pseudopotential^{97,98} was employed on the oxygen atoms in all calculations. The Hartree-Fock and Becke3LYP calculations were carried out using the 6-31(3+)G contracted Gaussian-type basis set of Ref. 81 on the H atoms and a *4s5p2d* contracted Gaussian-type basis set on the O atoms. The latter basis set was formed by adding two *d* functions, with exponents of 0.80 and 0.332, to the Stuttgart ECP basis set for oxygen.⁹⁹ For both isomers **A** and **B**, the Hartree-Fock method underbinds the excess electron, while the Becke3LYP method overbinds it.

The wave functions and the configurations from the VMC calculations were used to carry out the DMC calculations in the fixed-node approximation.⁸⁶ Due to the diffuse nature of the orbital occupied by the excess electron, errors caused by the fixed-node approximation are expected to be nearly the same for the neutral and anionic clusters, and thus, should largely cancel in the EBEs.^{37,100} The trial wave functions were generated using the Gaussian 03 program,¹⁰¹ and the VMC and DMC calculations were performed using the CASINO code.¹⁰² The DMC simulations were run using 4000 walkers, with 200000-300000 Monte Carlo steps per walker, and for time steps of 0.003, 0.004, and 0.005 au. The results from the different time steps were used to extrapolate the energies to 0 time step.⁸⁵

5.3 RESULTS

The total energies of the neutral and anionic clusters of isomer **A** obtained using the various methods are given in Table 5.1, and the corresponding results for isomer **B** are reported in Table 5.2. For isomer **A**, the DMC total energies obtained using the Hartree-Fock trial wave functions

are, within statistical errors, the same as those obtained using the Becke3LYP trial wave functions, indicating that essentially the same nodal surfaces are obtained for the two types of trial wave functions. For isomer **B** the DMC calculations using the Hartree-Fock trial wave functions give somewhat higher (~ 0.014 au) total energies for both the neutral and anionic clusters than do the DMC calculations using the Becke3LYP trial wave functions, indicating that the B3LYP trial functions provide slightly better representations of the nodal surfaces in this case.

Table 5.1 Total energies (au) of the neutral and anion of A

Methods	Anion	Neutral
HF	-100.8067	-100.7961
B3LYP	-102.7771	-102.7520
VMC-HF	-102.805(5)	-102.788(5)
VMC-B3LYP	-102.569(7)	-102.557(5)
DMC-HF	-103.244(2)	-103.226(2)
DMC-B3LYP	-103.240(2)	-103.224(2)

Table 5.2 Total energies (au) of the neutral and anion of B

Methods	Anion	Neutral
HF	-100.7475	-100.7445
B3LYP	-102.7184	-102.6789
VMC-HF	-102.420(7)	-102.404(7)
VMC-B3LYP	-102.565(7)	-102.555(7)
DMC-HF	-103.175(3)	-103.147(2)
DMC-B3LYP	-103.189(2)	-103.162(3)

The electron binding energies are summarized in Table 5.3. For isomer **A** the DMC calculations with the HF and B3LYP trial wave functions give EBEs of 0.49 ± 0.08 and 0.44 ± 0.08 eV, respectively, in excellent agreement with the CCSD(T) result of 0.47 eV. For **B** the DMC calculations with the HF and B3LYP trial wave functions give EBEs of 0.76 ± 0.10 and 0.73 ± 0.10 eV, respectively, again in excellent agreement with the CCSD(T) result of 0.78 eV. Most strikingly, even though the Hartree-Fock method drastically underbinds the excess electron for structure **B**, the DMC procedure is able to recover from this deficiency. For **B** the underbinding of the excess electron in the Hartree-Fock approximation is greater in the present study than found in Ref. 78. This is primarily a consequence of the neglect of p functions on the H atoms in the basis set employed in the present study. To check whether this deficiency of the atomic basis set impacts the EBE calculated with the DMC method, we have also carried out calculations for structure **B** using a HF trial function generated using an expanded basis set formed by adding to the basis set described above two p functions (from the aug-cc-pVDZ basis set¹⁰³) to each H atom. This expanded basis set gives the same Hartree-Fock value of the EBE of **B** as reported in Ref. 77. Moreover, the DMC/HF calculations with the expanded basis set give nearly the same value of the EBE as of both the neutral and anionic species are lowered in energy by early the same extent (~ 0.024 au). Thus the DMC method is also very effective at overcoming limitations in the atomic basis set. Most noteworthy is the finding that with the larger basis set, the statistical errors in the total energies of **B** are considerably reduced, with the result that the statistical uncertainty in the EBE is only 0.04 eV.

From Table 5.3 it is seen that for both structures **A** and **B**, the MP2 values of the EBEs are, in fact, quite close to the CCSD(T) values. It should be noted, however, that there are other

arrangements of water molecules, for which the CCSD(T) values of the EBEs are much larger than the MP2 values,¹⁰⁴ and for which the DMC approach would be especially advantageous.

Table 5.3 Electron binding energies (EBE) (ev) of species A and B

Methods	A	B
HF^a	0.29 (0.29)	0.08 (0.26)
B3LYP	0.68	1.07
MP2^a	0.40	0.75
CCSD(T)^a	0.47	0.78
VMC-HF	0.46±0.19	0.44±0.27
VMC-B3LYP	0.33±0.23	0.27±0.27
DMC-HF	0.49±0.08	0.76±0.10
DMC-B3LYP	0.44±0.08	0.73±0.10

^a The MP2 and CCSD(T) EBEs of **A** and **B** are from Ref. 78. The Hartree-Fock results given in parenthesis are also from Ref. 78

In this study we have shown that DMC calculations using either Hartree-Fock or Becke3LYP trial wave functions give for the $(\text{H}_2\text{O})_6^-$ cluster electron binding energies in excellent agreement with the results of large basis set CCSD(T) calculations. Comparable quality CCSD(T) calculations would be feasible for $(\text{H}_2\text{O})_7^-$ and $(\text{H}_2\text{O})_8^-$ but would be computationally prohibitive on still larger water clusters. On the other hand, DMC calculations, with their n^3 scaling and high degree of parallelization, should be applicable to $(\text{H}_2\text{O})_n^-$ clusters with n as large as 30. The finding that the diffusion Monte Carlo method gives nearly the same EBEs with the Hartree-Fock and B3LYP trial wave functions is important as it means that one can confidently employ B3LYP trial wave functions in cases where the Hartree-Fock procedure fails to bind the excess electron.

6.0 THE QMC STUDY OF THE WATER-ACENE SYSTEMS

6.1 INTRODUCTION

The interactions between water and acene compounds are of fundamental importance in many research areas. In material science and technology, this is partly associated with the practical interest in carbon nanotubes (CNT), which have much promise in biosensor technology and other applications involving water^{105,106}. A number of fundamental studies of the interactions water-acenes systems also aimed at exploring the structural and phase behavior of water at the nanometer scale⁵. Many properties of biological systems such as the structure of proteins, the structure and function of biopolymers, and molecular recognition processes are influenced by the interactions between acene molecules and water¹⁰⁷.

Water can interact with acene molecules in several ways. Both H atoms and the O nonpaired electrons in H₂O can participate in forming bonds between molecules. Most acene compounds are immiscible in water, which indicates that the magnitudes of the interactions between water and aromatic molecules are very weak.

Weak interactions possess a key role in physics and chemistry. Their respective strengths determine the melting and boiling points as well as solvation energies and the conformation of large biomolecules. The term “weak interactions” is the combined effect of electrostatic repulsion or attraction, exchange repulsion, and dispersion attraction. Therefore a theoretical

treatment of the weak interactions requires an equally good and balanced description of each of these effects.

Electrostatic interactions and exchange repulsion are in most cases sufficiently accurately obtained with mean-field approaches such as Hartree-Fock (HF) and current implementations of Kohn-Sham density-functional theory (DFT), but dispersion interactions on the other hand originate from the correlated movement of electrons and are therefore not present in the HF picture. DFT methods with a dispersion component seem to cover some dispersion interaction, but unfortunately the performance is “far from generally applicable” and “having to be tailored to the problem in question”^{19,108}

The second-order Møller-Plesset perturbation (MP2) method and coupled cluster (CC) method can perform high accuracy to study the dispersion interactions. However they are slowly convergent and scale badly with system size. They also suffer from basis set superposition error, basis set incompleteness error, and the linear dependency error when using large basis set for large systems⁶. In a certain sense the QMC method appears like a natural choice for the theoretical treatment of the weak interactions in water-acene systems.

6.2 THE QMC STUDY OF THE WATER-BENZENE COMPLEX WITH ALL-ELECTRON TRIAL FUNCTIONS

6.2.1 Introduction

Benzene has the simplest structure of the acene family. An accurate treatment of this prototype system is important for studying more complex water-acene systems. Many theoretical and

experimental investigations have been done for the benzene-water complex. Suzuki et al. first indicated that benzene can form weak hydrogen bonds with water¹⁰⁹. The typical hydrogen bond is stronger than the van der Waals bond but weaker than covalent or ionic bonds.

Experimentally, the rotationally resolved spectra of the benzene-water complex showed that the water molecule is positioned above the benzene plane with both H atoms pointing toward one face of the benzene, indistinguishably^{109,110}. Although the H positions were not directly located in those experiments, they provided strong evidence for an interaction between the proton donors (H atoms in water) and the proton acceptors (the benzene π cloud). From a theoretical point of view, MP2 and CCSD(T) calculations show that, the most stable configuration for the water-benzene system is that of water positioned above the center of the benzene ring with a single H atom pointing toward the benzene and the other pointing away from it^{111,112}. However, The energy difference between these two configurations is very small^{108,113}.

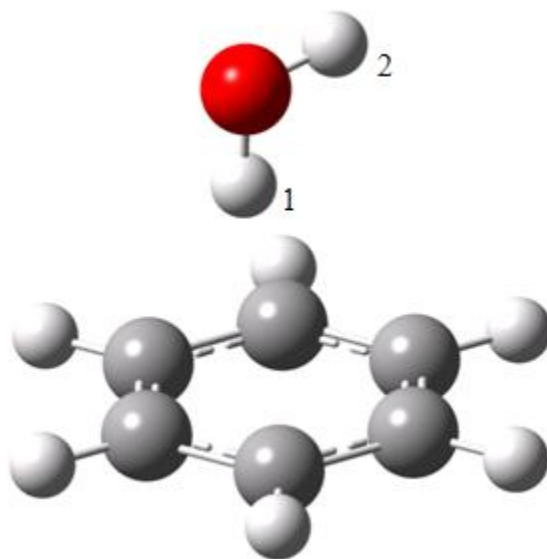


Figure 6.1 MP2-optimized global minimum structure of the water-benzene complex

6.2.2 Computational details

Figure 6.1 shows the geometry of the water-benzene complex which was used in our QMC calculations. It is given by the MP2/6-31+G[2d,p] optimization, which is close to those obtained from MP2 and CCSD(T) calculations with larger basis sets¹¹². The optimized geometry of the benzene monomer agrees well with the experiment data: $r_{CC}=1.397$ Å, and $r_{CH}=1.084$ Å¹¹⁴. The interaction of the water monomer with the benzene ring causes the two OH bond lengths to become unequal. One of the OH bonds is 0.967Å, in which the H atom π -bonded to the benzene ring. The other one is 0.964Å, which is about 0.003 Å shorter than the π -bonded one, and 0.007 Å longer than the experimental one, 0.957 Å⁶⁶. For the benzene-water complex, the predicted distance between the water and benzene centers of mass is 3.210 Å, which is considerably shorter than the experimental values ranging from 3.32 to 3.35 Å. However, it is very close to Feller's MP2 result with larger basis set, 3.211Å. The distance from the center of the benzene ring to the hydrogen atom involved in the hydrogen bond is 2.306 Å in our calculation. This value is about 0.007 Å short than the distance at the MP2/aug-cc -pVTZ level reported by Feller¹¹².

Table 6.1 Equilibrium Dissociation Energy of the water-benzene system from various *ab initio* methods

Method	De (kcal/mol)
MP2/6-31+G[2d,p] ¹¹¹	-2.83
MP2/CBS ¹¹²	-3.9±0.2
MP2/CBS ¹¹⁵	-3.61
CCSD(T)/CBS ¹¹⁵	-3.28
DMC/HF/6-311++G**	-3.4±0.3

6.2.3 Results

Table 6.1 shows our result for the dissociation energy from DMC calculations with HF/6-311++G**trial wave functions, which is -3.4 ± 0.3 kcal/mol. Fredericks and Jordan reported that the dissociation energy of the water-benzene complex was -2.83 kcal/mol from the MP2 calculations using the 6-31+G[2d,p] basis set¹¹¹. Feller proposed the MP2 complete basis set (CBS) limit dissociation energy, $E_{\text{MP2(CBSlimit)}}$, as -3.9 ± 0.2 kcal/mol from the average of the BSSE corrected $E_{\text{MP2(CBSlimit)}}$, -3.7 kcal/mol and the BSSE not corrected MP2/cc-pVQZ interaction energy of 4.1 kcal/mol¹¹². Feller also reported that the MP2 calculations slightly overestimate the attraction (0.2 - 0.3 kcal/mol) compared to the CCSD(T) calculations using the aug-cc-pVDZ and aug-cc-pVTZ basis sets¹¹². Jurecka *et al.* also reported the $E_{\text{MP2(CBSlimit)}}$ and $E_{\text{CCSD(CBSlimit)}}$ complete basis set (CBS) limit dissociation energies as -3.61 kcal/mol and -3.28 kcal/mol, respectively¹¹⁵.

The change in vibrational zero point energy (ZPE) for the reaction $\text{C}_6\text{H}_6\text{-H}_2\text{O} \rightarrow \text{C}_6\text{H}_6 + \text{H}_2\text{O}$ can be obtained from normal-mode analyses, and amounts to 1.0 kcal/mol¹¹². Adding this to our DMC electronic dissociation energy, yields $\Delta E_0(0 \text{ K}) = -2.4 \pm 0.3$ kcal/mol, in good agreement with the experimental value of $\Delta E_0(0 \text{ K}) = -2.25 \pm 0.28$ kcal/mol¹¹⁶, and $\Delta E_0(0 \text{ K}) = -2.44 \pm 0.09$ ¹¹⁷.

An analysis of the time-step dependence of the equilibrium dissociation energy of the water-benzene system for the DMC/ HF-6-311++G** calculations was performed. The result is shown in Figure. 6.2. The time step errors in the monomer (water or benzene) and the water-benzene complex calculations cancel a lot at small time steps. However, energy extrapolations to

0 time step for the monomers and the dimer are necessary for obtaining accurate electronic dissociation energy of the water-benzene system.

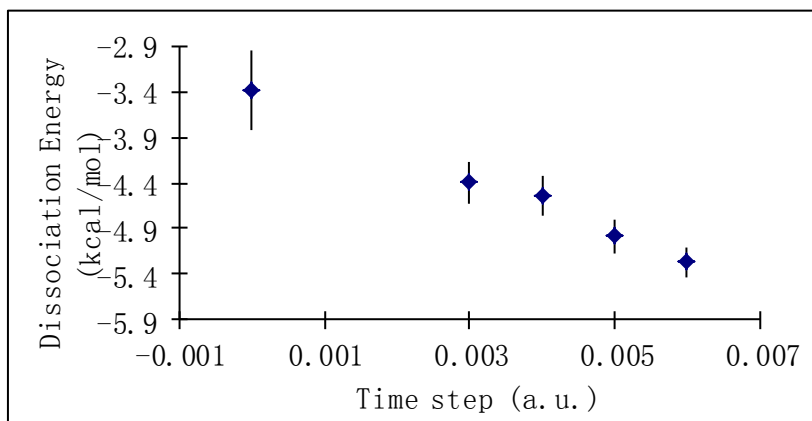


Figure 6.2 Time-step dependence of the equilibrium dissociation energy of the water-benzene system for the DMC/ HF-6-311++G** calculations

6.3 THE QMC STUDY OF THE WATER-ANTHRACENE COMPLEX WITH PSEUDOPOTENTIAL

6.3.1 Introduction

Different from the benzene–water complex, which is well studied both experimentally and theoretically, seldom experimental or theoretical data exist on the water-anthracene complex. From a theoretical point of view, the water-anthracene system is too complex for MP2 and CCSD methods with large enough basis set to give an accurate dissociation energy.

We performed pseudopotential QMC calculations of the water-anthracene system using Slater-Jastrow wave functions with Hartree-Fock orbitals. The use of pseudopotentials in QMC may introduce an additional source of error, the localization approximation. However, there are several advantages to use pseudopotentials in the QMC calculations. One of the advantages of using pseudopotentials is that they avoid the short-range variations in the wave function near the nuclei, and hence the energy fluctuations will be largely reduced. It was also suggested that the core electrons are responsible for much of the time-step bias¹¹⁸. The time-step bias remains small up to much larger time steps in the pseudopotential calculations. Thus we can use a larger time step region, in which the trend of the energy extrapolation is still nearly linear, in pseudopotential calculations than that in all electron calculations. It was verified in our DMC calculations of the water-anthracene system (See Figure. 6.3). The pseudopotentials we used are from the CASINO pseudopotential library^{119,120}. These pseudopotentials have been found to work very well in conjunction with QMC methods^{61,121}.

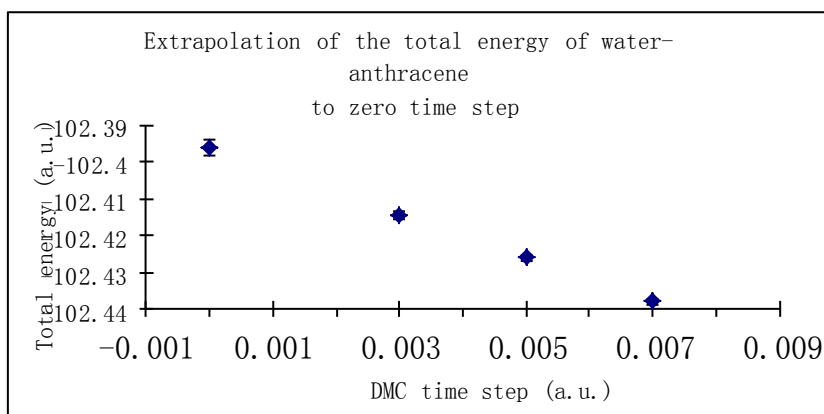


Figure 6.3 DMC energy of the water-anthracene complex as a function of the time step

6.3.2 Computational details

Figure 6.4 shows the geometry of the water-anthracene complex, which was used in our calculation. It is given by the MP2/aug-cc-pvdz optimization. For the anthracene monomer, $r_{CC} = 1.452 \text{ \AA}$, and $r_{CH} = 1.046 \text{ \AA}$. For the water monomer, the experimental equilibrium geometry⁶⁶ was used, $r_{OH} = r'_{OH} = 0.9572 \text{ \AA}$ and $\angle_{HOH} = 104.52^\circ$. For the water-anthracene complex, the predicted distance between the water and anthracene centers of mass is 3.137 \AA . The distance from the center of the anthracene face to the hydrogen atom involved in the hydrogen bond is 2.370 \AA .

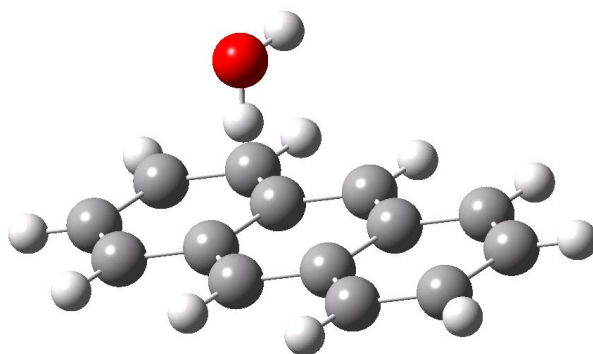


Figure 6.4 MP2-optimized structure of the water-anthracene complex

Table 6.2 Equilibrium Dissociation Energy of the water-anthracene system

Method	D_e (kcal/mol)
SAPT/aug-cc-pVTZ ¹²²	-2.9
LMP2/aug-cc-pVTZ(-f) (CP) ¹²³	-3.0
DMC/HF-Pseudopotential	-4.3 ± 1.8

6.3.3 Results

Table 6.2 shows the result of the dissociation energy of the water-anthracene complex from the pseudopotential DMC calculations with HF trial wave functions. We obtain a lower equilibrium dissociation energy of DMC/HF-Pseudopotential than that of SAPT and LMP2 methods with aug-cc-pVTZ basis set, although this value is still within the error bars. It should be noted that the dissociation energy of the water-benzene system of LMP2/aug-cc-pVTZ(-f) (CP) method was reported as -2.64 kcal/mol, which is 0.36 kcal/mol higher than that of the water-anthracene system of LMP2/aug-cc-pVTZ(-f) (CP) method¹²³. The same trend, that the dissociation energy of the water-anthracene system was lower than that of water-benzene system, was also reported by Feller and Jordan⁶. Since our DMC result for the water-benzene system quite agrees with the CCSD/CBS calculation and the experimental value, we suggested that the dissociation energy of the water-anthracene system should be around the region of -3.4~-4.3 kcal/mol.

6.4 THE QMC STUDY OF LARGE WATER-ACENE SYSTEMS USING LOCALIZED ORBITALS

6.4.1 Introduction

The QMC methods can give accurate studies for the water-benzene and water-anthracene systems. However, it is evident that “accuracy” is not the only one that we should seriously consider for water-anthracene and even larger water-ancene systems. The factor of “efficiency” becomes much more important for studying larger interacting systems. Although the QMC

methods is highly parallelizable, and adapted to a broad definition of parallel computers, it is still necessary to achieve better time scales of the QMC methods for studying large water-acene complexes.

In standard QMC, the orbitals are HF or DFT eigenfunctions extending over the entire system. Let the number of electrons in the system be N . The computational cost C of a standard QMC calculation is, $C = AN^3 + BN^4$, where the N^3 term comes from (i) evaluating all N single-particle orbitals and their derivatives at the N new electron positions (using localized basis functions such as Gaussians), to reach a given target variance σ^2 scaling as $O(N)$, (ii) evaluating the Jastrow factor, and (iii) evaluating the interaction energy. The N^4 contribution arises from the N updates of the matrix of cofactors, each of which takes a time proportional to N^2 , to reach a given target variance σ^2 proportional to N . Because B is of the order of 10^{-4} , the N^3 term dominates in practice²³.

The rate-determining step in most QMC calculations is the evaluation of the orbitals in the Slater wave function. If each of the N orbitals at the N electron positions is expanded in $O(N)$ basis functions (e.g. plane waves) then the time taken to evaluate the Slater wave function scales as $O(N^3)$. On the other hand, if a localized basis set such as a cubic spline representation is used then the time taken to evaluate each orbital is independent of system size, and hence the time taken to evaluate the wave function scales as $O(N^2)$ ¹²⁴. Finally, if the orbitals themselves are spatially localized and truncated then the number of nonzero orbitals to evaluate at each electron position is independent of system size, and so the time taken to compute the wave function is $O(N)$ ²⁷. Remembering the factor of N from a target error bar σ^2 , the computational cost for ‘localized’ QMC calculation scales as $O(N^2)$, which allowed QMC calculations to be performed for larger systems.

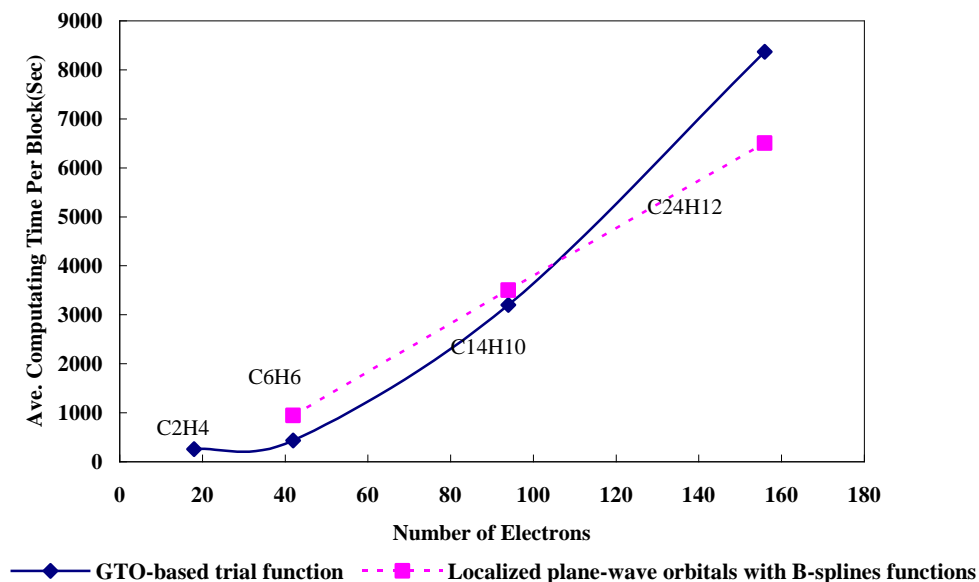


Figure 6.5 Computational cost of the DMC calculations for acene molecules as a function of the system size

6.4.2 Computational details and results

The QMC calculations with localized plane-wave orbitals represented as spline functions were performed to study benzene, anthracene, and coronene. The dash line in Figure 6.5 shows the results of the computational cost of the localized DMC calculations. The solid line is the results of the standard DMC calculations with Gaussian type orbitals for ethylene, benzene, anthracene, and coronene. For the acene molecules larger than anthracene, the localized DMC calculations won out in the competition. However, the localized orbital calculations do not offer a huge advantage due to: (1) localizing only the σ orbitals, and keeping π orbitals delocalized, and (2) the need to use larger localization radii for the larger acenes.

6.5 THE QMC STUDY OF THE WATER-BENZENE AND WATER-CORONENE COMPLEX WITH PSEUDOPOTENTIAL

6.5.1 Introduction

The interaction of molecules with acenes has attracted considerable interest for a variety of reasons, including the use of such systems as models for understanding molecular adsorption on graphene and graphite and for testing theoretical approaches for describing weak interactions. Of particular interest is the magnitude of the interaction of a water molecule with the graphene surface. This question has been addressed in numerous theoretical studies, with most of these concluding that the binding energy of a water molecule to a graphene sheet is about -3.1 kcal/mol.¹²⁵⁻¹²⁷ However, diffusion Monte Carlo (DMC)^{83-85,128} and random-phase approximation (RPA)¹²⁹⁻¹³¹ calculations give significantly smaller (in magnitude) binding energies (-1.6 and -2.3, respectively).¹³² In those studies using extrapolation of the results of calculations of water-acene systems to obtain the water-graphene limit, water-benzene and water-coronene systems play an important role.^{125,127} Based on the highest level calculations available for these systems, the binding energies of water-benzene and water-coronene are about -3.2 and -3.05 to -3.35 kcal/mol, respectively.^{125,127,133} In the case of water-benzene, the theoretical estimates are in excellent agreement with the values deduced from experiment, while there is no experimental value for the binding energy for the water-coronene system.

In extending electronic structure calculations to the larger acenes needed to realistically model water interacting with graphene, there are multiple challenges. Foremost among these is the fact that dispersion interactions play a major role in the binding.¹²⁷ As a result, traditional generalized gradient or hybrid density functional (DFT) methods are not suitable. This problem

is partially overcome by the use of dispersion-corrected DFT approaches. However, several such approaches were recently tested for water-coronene and none were found to give a quantitatively accurate description of the interaction potential.¹²⁷ The MP2 method^{134,135} does include dispersion interactions, but can overestimate their importance. Although this problem can be solved by use of the CCSD(T) method,¹³⁶⁻¹³⁸ this approach (as traditionally formulated) is computationally prohibitive for large acenes. In addition to the challenges posed by dispersion interactions, traditional quantum chemistry methods using Gaussian-type orbitals are plagued by near-linear dependency and basis set superposition error (BSSE)^{6,139} problems when applied to molecules interacting with large acenes. Two of the most promising methods for characterizing the interaction of water and other molecules with large acenes are DFT-based symmetry-adapted perturbation theory with density fitting (DF-DFT-SAPT)¹⁴⁰⁻¹⁴² and the MP2-C method of Hesselmann.^{143,144} There are two implementations of the former – the DF-DFT-SAPT approach of Hesselmann and co-workers¹⁴¹ and the DF-SAPT (DFT) method of Szalewicz and co-workers.^{140,142} These methods display $O(N^5)$ scaling, where N is the number of electrons, and are computationally attractive compared to CCSD(T). However, these approaches still suffer from near-linear dependency problems when flexible basis sets containing diffuse functions are employed. Moreover, the MP2, MP2C, and other methods that involve perturbative corrections to the Hartree-Fock wave function might not be appropriate for large acenes due to their small HOMO/LUMO gaps.

An alternative approach for calculating interaction energies, which is free of the problems described above, is the diffusion Monte Carlo (DMC) method.^{83-85,128} This method has already been applied to several weakly interacting systems, including water clusters^{37,145,146} and the water-benzene dimer.¹⁴⁷ In the usual fixed-node implementation,^{83,84} DMC calculations make use

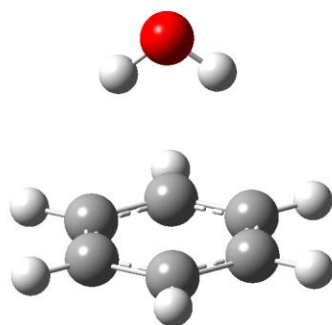
of trial function – generally a Slater determinant comprised of Hartree-Fock (HF) or DFT orbitals multiplied by a Jastrow factor⁹³ to describe the electron-electron, electron-nuclear, and electron-electron-nuclear correlations. DMC calculations afford the advantages of being relatively insensitive to the basis set used for the trial function and having a relatively low, $O(N^3)$ scaling, albeit with a large prefactor. The large prefactor is "compensated" by the fact that the DMC calculations are highly parallel.

In this section, we use the DMC method with HF trial wave functions to calculate the interaction energies of the water-benzene and water-coronene complexes. Water-benzene is included to establish an appropriate Gaussian basis set for describing the trial functions. Two different procedures for calculating the interaction energy are examined. One uses as the reference the DMC energies of the isolated monomers and the other a DMC calculation on the dimer with the two monomers far apart.

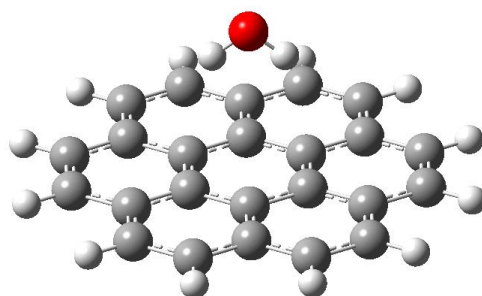
6.5.2 Computational Details

The structures of the water-benzene and water-coronene complexes considered in this study are shown in Figure 6.6. The geometries employed are the same as those used in Ref. 126. For both benzene and coronene, the experimental C-C bond length (1.420 Å) and C-C-C angles (120°) for graphite are employed.¹⁴⁸ The acene C-H bond lengths and C-C-H angles were taken to be 1.09 Å and 120°, respectively. The experimental gas-phase geometry is employed for the water monomer, i.e., the O-H bond lengths are 0.9572 Å and the H-O-H angle is 104.52 °.¹⁴⁹ The water molecule was placed above and perpendicular to the middle of the central ring, with both OH groups pointing towards the acene, and an oxygen-ring distance of 3.36 Å¹²⁷ as shown in Figure. 1. This distance came from an optimization of the geometry of water-coronene using the DF-

DFT-SAPT method.¹²⁷ The experimentally observed water-benzene complex has minimum energy structure with a "tilted" water molecule with one OH group pointed toward the center of the ring.¹⁵⁰ However, the energy difference between the one H-down minimum and the two H-down saddle point structure is less than 0.2 kcal/mol.^{131,151,152}



water-benzene



water-coronene

Figure 6.6 Geometrical structures of the water-benzene and water-coronene

The DMC calculations were carried out using single-determinant trial wave functions obtained from Hartree-Fock calculations, combined with a three-term Jastrow factor⁹³ to describe the electron-electron, electron-nuclear, and electron-electron-nuclear correlations. The parameters in the Jastrow factor were obtained by minimizing the local energy by means of variational Monte Carlo (VMC) calculations.⁹⁶ A Dirac-Fock pseudopotentials^{97,98} were employed on all atoms. The Hartree-Fock calculations were carried out using modified versions of the contracted Gaussian-type basis sets of Burkatzki, Filippi, and Dolg.¹⁵³ For water-benzene, three different basis sets were considered, the smallest of which (*A*) is the VDZ basis set Burkatzki et al. which employs a 2s1p basis set for the H atoms and a 2s2p1d basis set for the C and O atoms. The intermediate basis set (*B*) employs a 3s2p basis set for the H atoms and a 3s3p2d basis set for the C and O atoms, and was formed by adding the diffuse "aug" functions of the aug-cc-pVDZ basis set^{154,155} to *A*. The largest basis set (*C*) employs 3s3p, 3s3p2d, 4s4p3d, and 4s4p3d2f sets for acene-H, water-H, C, and O atoms, respectively. Basis set *C* was formed by adding to the ATZ basis set of Burkatzki et al. the diffuse functions from the aug-cc-pVTZ basis set,^{154,155} and omitting the *f* functions on the C atoms and the *d* functions on the acene H atoms. As discussed below, DMC calculations on water-benzene give, within statistical errors, the same interaction energy whether using basis set *A*, *B*, or *C* to represent for the trial function. Although the computational effort of each DMC move grows with the complexity of the basis set, the number of steps needed to achieve a specified convergence generally decreases as the basis set is made more flexible. Basis set *B* represents a reasonable compromise and was adopted for generating the trial function for water-coronene. However, linear dependency problems were

encountered in the Hartree-Fock calculations on water-coronene with this basis set, and to solve this problem the diffuse exponents were scaled by a factor of two.

The wave functions and the configurations from the VMC calculations were used to carry out the DMC calculations in the fixed-node approximation.^{83,84,86} The errors introduced by the fixed-node approximation should largely cancel when the binding energies are calculated.³⁷ The trial wave functions were generated using the Gaussian 03 program,¹⁰¹ and the VMC and DMC calculations were performed using the CASINO code.^{102,128}

As mentioned above, two strategies were employed to obtain the binding energy. In the first strategy (S1), the binding energy is calculated from the difference of energy of the water-acene complex and the sum of energies of isolated acene and water molecules. In the second strategy (S2), the energy of the water-acene complex at large separation is used in place of the sum of the energies of the monomers. In each case the energies of the individual species are extrapolated to the zero time step limit, and these extrapolated results are used to calculate the zero-time-step binding energies. Although the final interaction energies obtained by extrapolation to zero-time steps should not depend on which strategy is used, we are interested in determining whether the errors due to the use of finite time steps largely cancel in the S2 strategy, as this would allow for a reduction in the computational effort.

For the water-benzene complex time steps of 0.003, 0.005, and 0.007 au were used in the DMC calculations of the dimer, the isolated benzene molecule, and the isolated water molecule. For the water-coronene system the calculations were performed for time steps of 0.005, 0.007, and 0.01 au. The DMC simulations were run using total target populations of 4000-16000 walkers and a minimum of 70,000 Monte Carlo steps.

For the purpose of comparison, we also calculated the binding energy of water-coronene using the direct RPA method.¹⁵⁶ Three sets of RPA calculations were performed: (1) one using the HF approximation to describe the first-order electrostatics and exchange repulsion and using HF orbital to evaluate the RPA correlation energies, (2) using PBE¹⁵⁷ orbitals to evaluate the first-order electrostatics and exchange repulsion plus the RPA correlation corrections and (3) applying the single-excitation correction to the RPA/PBE results.¹⁵⁸ This last method is referred to as RPA-s/PBE. The RPA calculations were performed with the FHI AIMS code¹⁵⁹ using the tier 3 basis set.¹⁶⁰

6.5.3 Results

(a) Water-benzene

As seen from Table 6.3 and Figure 6.7, the binding energy of the water-benzene complex, when calculated using the S1 strategy, shows a strong (linear) dependence on the time step and, although the binding energies for basis sets *B* and *C* are significantly different at each time step, they extrapolate to similar values in the zero time step limit (-3.26 ± 0.26 and -3.01 ± 0.26 kcal/mol, respectively). The results with the smallest basis set *A*, are not reported in the Table, but they extrapolate to a value of -3.2 ± 0.3 kcal/mol, consistent with those obtained with DMC calculations using trial wave functions described with the larger basis sets.

Table 6.3 Total energy and binding energy of the water-benzene complex

methods ^a	water-benzene (3.36 Å)(au)	benzene (au)	water (au)	water- benzene (12 Å) (au)	binding energy (kcal/mol)
HF-B-S1	-53.31147	-36.43203	-16.87832	**	-0.70
HF-B-S2	-53.31147	**	**	-53.31040	-0.69
HF-C-S1	-53.37245	-36.47133	-16.89949	**	-1.02
HF-C-S2	-53.37245	**	**	-53.37086	-1.00
DMC-B-S1	-54.7807(2)	-37.5737(3)	-17.2018(2)	**	-3.26±0.26
DMC-B-S2	-54.7807(2)	**	**	-54.7756(3)	-3.20±0.21
DMC-C-S1	-54.8020(3)	-37.5880(2)	-17.2092(2)	**	-3.01±0.26
DMC-C-S2	-54.8020(3)	**	**	-54.7972(3)	-3.01±0.27
DMC ^b					-3.4±0.3
CCSD(T)/CBS ^c					-3.28
CCSD(T)/CBS ^d					-3.20
CCSD(T)-F12 ^e					-3.21
Experiment ^f (ZPE Corrected)					-3.25±0.28
Experiment ^g (ZPE Corrected)					-3.44±0.09

^a B: basis set B; C: basis set C; S1: strategy 1; S2: strategy 2.

^b MP2/6-31+G[2d,p] level optimized geometry with rigid monomer.

^c From Ref. 161.

^d From Ref. 132.

^e From Ref. 160.

^f From Ref. 163.

^g From Ref. 149.

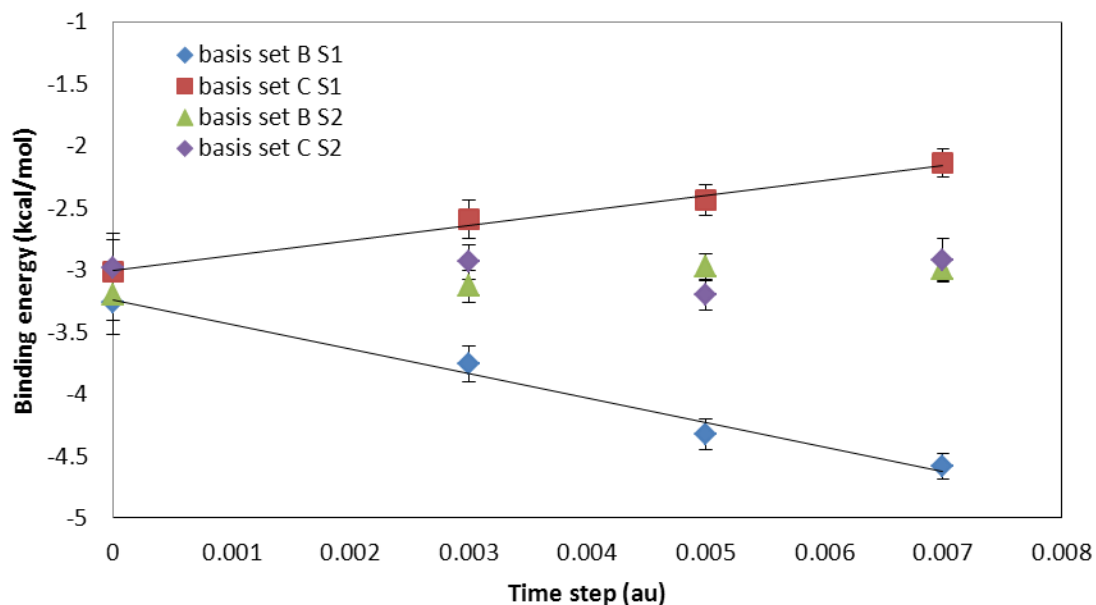


Figure 6.7 Binding energy of water-benzene from DMC calculations using strategies S1 and S2 and basis sets B and C

The binding energies obtained using the S1 and S2 procedures and extrapolation to the zero time step limit are essentially identical. In addition, with the S2 procedure most of the bias due to the use of finite time steps is removed from the result that, within the statistical errors, the same binding energy is obtained for each time step. This is most encouraging because it means that one can obtain accurate interaction energies by using the S2 procedure only a single time step. Moreover, a reasonably large value of the time step can be used reducing the computational time needed to achieve the desired convergence. With this approach, the computational effort can be reduced by about a factor of five compared to that required for the S1 procedure.

Our DMC values of the binding energy of water-benzene are in excellent agreement with that $(-3.21 \text{ kcal/mol})^{161}$ obtained from CCSD(T)-F12 calculations using the same geometry and

with complete basis set limit (CBS) CCSD(T) values, -3.20 and -3.28 kcal/mol,^{133,162} obtained for the structure with one OH down.¹³³ We also carried out DMC calculations for the water-benzene complex with the one OH group down structure using the MP2/6-31+G[2d,p] level optimized geometry, obtaining a value of -3.4 ± 0.3 kcal/mol for the binding energy. The vibrational zero-point energy correction to the dissociation energy of water-benzene has been estimated to be about 1.0 kcal/mol.^{133,163} Applying this correction to our DMC result for the MP2 optimized geometry we obtain a D_0 value of -2.4 ± 0.3 kcal/mol in excellent agreement with the experimental value of -2.44 ± 0.09 and -2.25 ± 0.28 kcal/mol.^{150,164}

(b) Water-coronene

The results for the water-coronene dimer are summarized in Table 6.4 and Figure 6.8. From comparison of Figures 6.7 and 6.8, it is seen that with the S1 procedure the time step errors are much greater for water-coronene than for water-benzene. However, with the S2 procedure, the water-coronene interaction energy is relatively insensitive to the time step. As for water-benzene, the interaction energy of water-coronene obtained from the two approaches - S1 with extrapolation to zero time step and S2 using individual time steps - agree to within the statistical errors. We take the S2 result with -0.007 au time step, -3.20 ± 0.28 kcal/mol, as our best estimate of the interaction energy between water-coronene at the employed geometry. (We choose this value rather than that obtained from the S1 procedure due to the smaller statistical error.)

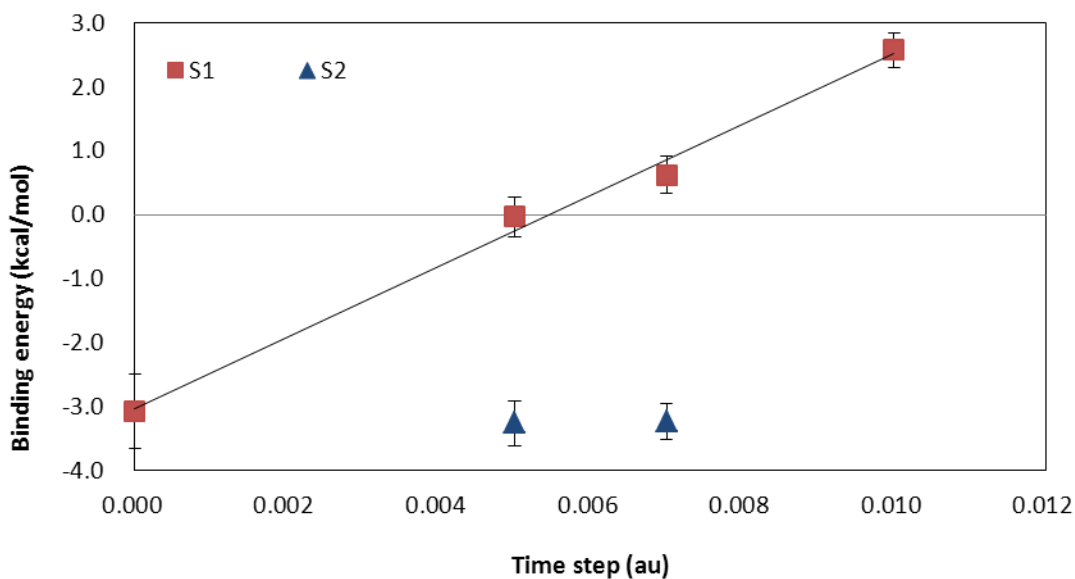
Table 6.4 Binding energy of the water-coronene complex

method ^a	water-coronene (au)	coronene (au)	water (au)	water-coronene (15 Å) (au)	Binding energy (kcal/mol)
HF-S1	-155.80389	-138.92435	-16.87836	**	-0.74
HF-S2	-155.80389	**	**	-155.80275	-0.71
DMC-S1	-160.4144(7)	-143.2075(7)	-17.2020(1)	**	-3.07±0.57
DMC-S2-T1	-160.4548(3)	**	**	-160.4497(3)	-3.20±0.28
DMC-S2-T2	-160.4438(4)	**	**	-160.4386(4)	-3.26±0.35
DF-DFT-SAPT ^b					-3.05
CCSD(T)/CBS ^c					-3.35

^aS1 involves separate calculations on the two monomers at different time steps and extrapolation to zero time step, while S2 uses a calculation on the dimer with a 15 Å separation between the water O and the center of the ring. T1: time step 0.007 au; T2: time step 0.005 au.

^bFrom Ref. 126.

^cFrom Ref. 124.

**Figure 6.8** Binding energy of water-coronene from DMC calculations using S1 and S2 strategies

We are unaware of any experimental values of the binding energy for the water-coronene dimer. Probably the most accurate prior theoretical estimates of this binding energy are -3.05 and -3.35 kcal/mol from DFT-SAPT¹²⁷ and CCSD(T)/CBS¹²⁵ calculations, respectively. Within the statistical error, the present DMC estimate of binding energy of water-coronene is consistent with these values. We note that direct RPA calculations using PBE orbitals give a binding energy of -2.5 kcal/mol (Table 6.5) when using the same geometry as employed for the DMC calculations. However, the RPA-s/PBE method which includes a correction for single excitations¹⁵⁸ gives a binding energy of -3.0 kcal/mol in close agreement with the DMC, DFT-SAPT, and CCSD(T) results.

Table 6.5 Binding energies (kcal/mol) of water-benzene, water-coronene, and water-graphene

	water-benzene	water-coronene	water-graphene
DMC	-3.2±0.2 ^a	3.2±0.3 ^a	-2.1 ^b
CCSD(T)	-3.2 ^c	-3.3 ^d	-3.1 ^e
DFT-CC	-3.2 ^f	-3.3 ^d	-3.1 ^d
DFT-SAPT	-3.2 ^g	-3.0 ^g	-3.0 ^{g, h}
RPA/HF	-2.4 ⁱ	-2.1 ^a	
RPA/PBE	-2.5 ⁱ	-2.5 ^a	-2.3 ^b
RPA-s/PBE	-2.9 ⁱ	-3.0 ^a	-2.8 ^j

^a Present study.

^b From Ref. 131. DMC value including correction for going from a single k-point to a suitable grid of k points.

^c From CCSD(T)/CBS calculations of Ref. 132.

^d From Ref. 124.

^e From Ref. 125. CCSD(T) result estimated using the incremental method.

^f From Ref. 150.

^g From Ref. 126.

^h Estimated from DFT-SAPT results for a series of water-acene systems.

ⁱ From Ref. 160.

^j Estimated as described in the text.

The present study and earlier studies^{127,152,161} indicate that the binding energies of water-acene systems are relatively insensitive to the size of the acene. At first sight this is surprising as one would expect the induction and dispersion contributions to the binding to grow with increasing size of the acene. However, as was observed in Refs. 126 and 151, the electrostatics contribution decreases in magnitude with increasing size of the acene, roughly compensating for the increasing magnitude of the dispersion contribution.

6.5.4 Conclusions

In this study, we demonstrate that the DMC method using a Hartree-Fock trial function gives binding energies for water benzene and water-coronene that are consistent with the best prior estimates of these quantities from *ab initio* calculations. It is found that the error due to the use of finite time steps can be mitigated by the use of a DMC calculation of the two monomers at large separation for obtaining the sum of the energies of the two non-interacting monomers. In light of this and the $O(N^3)$ scaling of DMC calculations, it would be possible to extend these calculations to water interacting with much larger acenes, for which it would be difficult, if not impossible, to obtain CCSD(T)/CBS results.

It was noted in the Introduction that a recent DMC calculation gave a value of -1.6 kcal/mol for the binding of a water molecule to the graphene surface.¹³² This value is about 1.4 kcal/mol smaller (in magnitude) than obtained in other recent theoretical studies of water-graphene.¹²⁵⁻¹²⁷ The DMC calculations of Ref. 131 were carried out using periodic boundary conditions, a single k point, and with a supercell containing 50 carbon atoms. Based on the

results of RPA calculations, the authors of Ref. 131 established that the error due to use of the Γ point only for k-point sampling is about 0.5 kcal/mol. Applying this correction to their DMC result gave a binding energy of -2.1 kcal/mol, which is still appreciably smaller in magnitude than other recent estimates of the binding energy of water-graphene. Possible remaining errors include the interactions between water molecules in adjacent cells and the inadequacy of a single determinant wave function for describing the nodal surfaces. Given the spacing between the water molecules, the error in the binding energy due to water-water interactions should be less than 0.2 kcal/mol. This suggests that the use of a single determinant trial function introduces an error of about 0.9 kcal/mol in the DMC value of the interaction energy for water-graphene. Ref. 131 also reported a RPA/PBE result of -2.26 kcal/mol for the water-graphene binding energy. However, we have found that the binding energy of water-coronene grows in magnitude from -2.5 to -3.0 kcal/mol in going from the RPA/PBE to the RPA-s/PBE method. This leads us to conclude that the RPA-s/PBE procedure would give a binding energy close to -2.8 kcal/mol for water-graphene, only slightly smaller in magnitude than the binding energies reported in Refs. 124, 125, and 126.

7.0 NEW GAUSSIAN BASIS SETS FOR QUANTUM MONTE CARLO CALCULATIONS

7.1 INTRODUCTION

Quantum Monte Carlo methods,^{83,84} because of their cubic scaling with the number of atoms, hold considerable promise for providing accurate interaction energies of molecular clusters. Most quantum Monte Carlo electronic structure calculations make use of the fixed-node approximation^{29,84} to enforce fermionic behavior on the wave function. The fixed nodal surface is enforced by a trial function, generally taken to be a single Slater determinant of Hartree-Fock or DFT orbitals, multiplied by the Jastrow factors⁹³ to describe electron-electron and electron-nuclei cusps. The parameters in the Jastrow factors are optimized by the use of the variational Monte Carlo (VMC) procedure. The VMC step is generally followed by diffusion Monte Carlo (DMC) calculations, which is where most of the computational effort is spent. The orbitals in the trial functions used in quantum Monte Carlo calculations are most frequently represented in terms of plane-wave or Gaussian-type orbitals (GTOs). In the former case, use of pseudopotentials is essential to avoid the prohibitively high plane-wave cutoffs that would be required for all-electron calculations. Moreover, even when using GTO basis sets, it is advantageous to use pseudopotentials in quantum Monte Carlo calculations as this greatly reduces the computational effort to achieve small statistical errors.

In our applications of quantum Monte Carlo methods employing trial functions expressed in terms of GTOs and employing pseudopotentials, we observed surprising large variances of the VMC energies. In some cases the variances were as much as a factor of six larger than obtained with high cut-off plane-wave basis sets.^{165,166} This naturally raises concern about the impact of such trial functions on the interaction energies obtained from subsequent DMC calculations. This concern has led us to design for O, C, and H correlation-consistent GTO basis sets for use with the Casino Dirac-Fock pseudopotentials.^{97,98} In this work we present these new correlation constant basis sets to evaluate their performance in VMC and DMC calculations. In addition, we examine the performance of two methods that have been designed for dealing with the problems associated with using non-local pseudopotentials in quantum Monte Carlo calculations.

7.2 VMC CALCULATIONS

To illustrate the nature of the large variance problem when using certain GTO basis set/pseudopotential combinations, we summarize in Table 7.1 the energies and variances from VMC calculations on the water molecule using the Casino Dirac-Fock pseudopotential on the H and O atoms and with the molecular orbitals in the trial functions represented either by the pVDZ GTO basis set of Burkatzki, Filippi, and Dolg (BFD)¹⁵³, augmented with diffuse of *s*, *p*, and *d* functions from the aug-cc-pVDZ basis set,^{154,155} or by plane-wave basis sets with energy cutoffs of 60, 120, and 160 a.u.. The geometry of the water monomer was taken from experiment,¹⁴⁹ with OH distances of 0.9572Å and an HOH angle of 105.52°. In the calculations using the GTOs, the trial wave function was taken from Hartree-Fock calculations, and in the calculations with the plane-wave basis set, the orbitals for the trial function were taken from local density

approximation (LDA) density functional theory calculations, with the orbitals being converted to BLIP-type spline functions.¹⁶⁷ In separate calculations using the augmented BFD basis set, we confirmed that the energy and variance from the VMC calculations are nearly the same whether using trial functions expanded in terms of Hartree-Fock or LDA orbitals. In all calculations, three-term Jastrow factors were employed, the parameters in which were optimized so as to minimize the variance of the energy. The Hartree-Fock calculations were carried out using the Gaussian 03 package,¹⁶⁸ and the DFT plane-wave calculations were carried out using ABINIT.¹⁶⁹ The quantum Monte Carlo calculations were carried out using the CASINO code.¹²⁸ The calculations with the augmented BFD GTO basis set give a variance of 1.25 a.u. compared with variances of 1.63, 0.34, and 0.26 a.u. obtained using plane-wave basis sets with cutoffs of 60, 120, and 160 a.u., respectively.

Table 7.1 VMC energies and variances for the water monomer using the Casino Dirac-Fock pseudopotential on all atoms^a

Basis set	VMC energy (a.u.)	Variance of the VMC energy (a.u.)
Augmented BFD	-17.161(3)	1.25
Plane-wave/BLIP (60 a.u.) ^b	-17.159(5)	1.63
Plane-wave/BLIP (120 a.u.) ^b	-17.191(2)	0.34
Plane-wave/BLIP (160 a.u.) ^b	-17.194(2)	0.26

a. The molecular orbitals for the GTO and plane-wave basis sets were obtained from Hartree-Fock and LDA calculations, respectively.

b. The plane-wave cutoff is given in parentheses.

Adding higher angular momentum functions to the augmented BFD GTO basis set had little effect on the variance. This led us to examine the variances obtained in all-electron VMC calculations using Dunning's cc-pVDZ, cc-pVTZ, cc-pVQZ, cc-pV5Z, and cc-pV6Z basis sets,¹⁵⁵ omitting *g* and higher angular momentum functions, as these are not supported by the

Casino code. The variances of the VMC energy for the above sequence of basis sets are 3.6, 2.4, 1.5, 1.1, and 0.8 a.u., respectively. Similar variances are obtained with the corresponding aug-cc-pVXZ basis sets basis sets.^{154,155} Due to the large contribution of the $1s$ electrons to the total energies, the variance in the complete basis set limit is necessarily larger in all-electron than in pseudopotential calculations. These results suggested that the large variance found in the VMC calculations with the extended augmented BFD basis set is due to the fact that this basis set is far from optimal for use with Casino Dirac-Fock pseudopotential. Although high quality aug-cc-pVXZ- type basis sets for use with pseudopotentials have been developed for heavier elements,¹⁷⁰⁻¹⁷² such basis sets have not been developed for Li-Ne, primarily due to the fact that with traditional quantum chemistry methods, there is little computational advantage to replacing the $1s$ orbitals by pseudopotentials. However, as noted above, the use of pseudopotentials to model the $1s$ electrons of Li-Ne is more advantageous in quantum Monte Carlo calculations. With this in mind, we have designed a series of correlation consistent basis sets for oxygen and carbon with the core $1s$ electrons described by Casino Dirac-Fock pseudopotentials. In addition, to facilitate comparison with calculations employing trial functions expressed in terms of plane-wave basis sets, we also developed analogous basis sets for use with the Casino Dirac-Fock pseudopotential for hydrogen. These basis sets are designated as aug-cc-pVDZ (CDF), aug-cc-pVTZ (CDF), aug-cc-pVQZ (CDF), and aug-cc-pV5Z (CDF) and are described in Table 7.2-7.4.

Table 7.2 aug-cc-pVXZ basis sets for oxygen in Gaussian09 format

Aug-cc-pVDZ	Aug-cc-pVTZ	Aug-cc-pVQZ	Aug-cc-pV5Z
S 4 1.0	S 6 1.0	S 8 1.0	S 10 1.0
11.4406 0.08363	10.1546 0.096389	18.84472 -0.029516	58.03297 -0.002591
7.27416 -0.207273	6.37 -0.283037	11.79099 0.182223	36.23793 0.01985
0.95278 0.573366 0.29088	3.98674 0.050966	7.3841 -0.360446	22.65517 -0.082116
0.541479	1.79565 0.128286	4.6178 0.167268	14.16847 0.208792

S 1 1.0			0.72768	0.587155	2.88657	-0.193426	8.7684	-0.245096		
	0.29088	1.0								
S 1 1.0			0.25211	0.413898	1.69534	0.312394	3.44237	-0.084054		
	0.0888	1.0	S 1 1.0		0.61236	0.592491	2.30015	0.109763		
P 4 1.0				1.79565	1.0	0.22118	0.324558	0.96585	0.423202	
	7.5686	0.107913	S 1 1.0		0.25211	S 1 1.0		0.40557	0.488075	
	2.4382	0.260983		1.0		1.69534	1.00	0.1703	0.16071	
	0.86732	0.440022	S 1 1.0			S 1 1.0		S 1 1.0		
	0.26935	0.421942		0.0873	1.0			2.30015	1.00	
P 1 1.0			P 6 1.0			S 1 1.0		S 1 1.0		
	0.26935	1.0		16.73989	-0.019406			0.96585	1.00	
P 1 1.0				10.48574	0.082373	S 1 1.0		S 1 1.0		
	0.0727	1.0		4.00777	0.127921			0.40557	1.00	
D 1 1.0				1.74357	0.287838	P 8 1.0		S 1 1.0		
	1.21925	1.0		0.64569	0.451838			0.1703	1.00	
D 1 1.0				0.20487	0.313232			S 1 1.0		
	0.3269	1.0	P 1 1.0					0.0715	1.00	
				0.64569	1.0			P 10 1.0		
			P 1 1.0					53.20848	-0.001496	
				0.20487	1.0			33.08254	0.009418	
			P 1 1.0					20.59562	-0.035314	
				0.0581	1.0			12.88695	0.06608	
			D 1 1.0					5.61128	0.086196	
				2.32444	1.0	P 1 1.0		3.51864	0.016914	
			D 1 1.0					2.20676	0.245761	
				0.65656	1.0			0.8669	0.386175	
			D 1 1.0					0.34056	0.340201	
				0.2053	1.0			0.16354		
			F 1 1.0					1.00	0.13378	0.136243
				1.42299	1.0			0.0538	1.00	
			F 1 1.0						2.20676	1.00
				0.4847	1.0	D 1 1.0				
								0.8669	1.00	
								P 1 1.0		
								0.34056	1.00	
								P 1 1.0		
								0.44532	1.00	
									0.13378	1.00

		D 1 1.0		P 1 1.0
		0.1469 1.00		0.0471 1.00
		F 1 1.0		D 1 1.0
		2.61391 1.00		5.31609 1.00
		F 1 1.0		D 1 1.0
		0.85131 1.00		2.14461 1.00
		F 1 1.0		D 1 1.0
		0.3128 1.00		0.86518 1.00
		G 1 1.0		D 1 1.0
		1.83814 1.00		0.34903 1.00
		G 1 1.0		D 1 1.0
		0.6998 1.00		0.1236 1.00
				F 1 1.0
				4.01865 1.00
				F 1 1.0
				1.56803 1.00
				F 1 1.0
				0.61183 1.00
				F 1 1.0
				0.2306 1.00
				G 1 1.0
				3.22935 1.00
				G 1 1.0
				1.18195 1.00
				G 1 1.0
				0.4938
				1.00
				H 1 1.0
				2.29924 1.00
				H 1 1.0
				1.0069 1.00

Table 7.3 aug-cc-pVXZ basis sets for hydrogen in Gaussian09 format

Aug-cc-pVDZ	Aug-cc-pVTZ	Aug-cc-pVQZ	Aug-cc-pV5Z
S 4 1.0	S 5 1.0	S 6 1.0	S 8 1.0
13.01 0.018161	33.87 0.003021	82.64 -0.000376	402 0.000022
1.962 0.140114	5.095 0.048453	12.41 0.016339	60.24 -0.000597
0.4446 0.476695	1.159 0.199653	2.824 0.075323	13.73 0.013185
0.122 0.501665	0.3258 0.506418	0.7977 0.257107	3.905 0.043733

S 1 1.0			S 1 1.0	0.1027	0.382386			0.2581	0.497216			1.283	0.143398
	0.122	1.00	S 1 1.0	0.3258	1.00	S 1 1.0		0.08989	0.296149			0.4655	0.329949
S 1 1.0			S 1 1.0			S 1 1.0		0.7977	1.00			0.1811	0.43703
	0.0297	1.00	S 1 1.0	0.1027	1.00	S 1 1.0				S 1 1.0		0.07279	0.176123
P 1 1.0			S 1 1.0			S 1 1.0		0.2581	1.00			1.283	1.00
	0.7364	1.00	P 1 1.0	0.0254	1.00	S 1 1.0		0.08989	1.00			0.4655	1.00
P 1 1.0			P 1 1.0	1.4452	1.00	S 1 1.0		0.0236	1.00			0.1811	1.00
	0.1419	1.00	P 1 1.0	0.3902	1.00	P 1 1.0		2.7109	1.00			0.07279	1.00
			D 1 1.0	0.1009	1.00	P 1 1.0		0.8905	1.00			0.0207	1.00
			D 1 1.0	1.0762	1.00	P 1 1.0		0.2925	1.00			4.6782	1.00
				0.2499	1.00	P 1 1.0		0.0833	1.00			1.7361	1.00
						D 1 1.0		1.9684	1.00			0.6443	1.00
						D 1 1.0		0.6364	1.00			0.2391	1.00
						D 1 1.0		0.1822	1.00			0.0725	1.00
						F 1 1.0		1.5518	1.00			3.2691	1.00
						F 1 1.0		0.3759	1.00			1.2524	1.00
												0.4798	1.00
												0.1498	1.00
												2.52	1.00
												0.9124	1.00
												0.2781	1.00
												2.2151	1.00
												0.5390	1.00

Table 7.4 aug-cc-pVXZ basis sets for carbon in Gaussian09 format

Aug-cc-pVDZ	Aug-cc-pVTZ	Aug-cc-pVQZ	Aug-cc-pV5Z
S 4 1.0	S 6 1.0	S 8 1.0	S 10 1.0
6.03476	11.57792	19.59101	31.36778
0.081605	-0.017912	0.007338	-0.002416
3.80212	7.2305	12.2387	19.53784
-0.206235	0.083429	-0.046054	0.018709
0.48701	3.57462	7.18672	12.19126
0.569109	-0.208471	0.170523	-0.078337
0.15251	0.933	4.49651	7.6152
0.542776	0.126287	-0.238316	0.201296
S 1 1.0	0.37693	1.4262	-0.229367
	0.587742	-0.097824	4.75817
	0.1329	0.8416	-0.088946
	0.418306	0.28021	1.92263
S 1 1.0	S 1 1.0	S 1 1.0	S 1 1.0
	0.933	0.3132	1.1955
	1.00	0.594111	0.094083
		0.1165	0.403249
P 4 1.0	S 1 1.0	S 1 1.0	S 1 1.0
	0.1329	0.8416	0.218
	1.00	1.00	0.50158
			0.0931
	0.0469	0.3132	0.172148
	1.00	1.00	
P 1 1.0	P 6 1.0	S 1 1.0	S 1 1.0
	7.89344	0.1165	1.1955
	-0.019146	1.00	1.00
	4.92416	0.0434	0.5105
	0.08135	1.00	1.00
	2.11811	0.0434	0.218
	0.093266		1.00
	0.99366	P 8 1.0	S 1 1.0
	0.25311		
	0.3817	14.28983	0.0931
	0.451298	0.004438	1.00
D 1 1.0	0.1284	8.93365	S 1 1.0
	0.360747	-0.031624	
		5.58553	0.0397
D 1 1.0	P 1 1.0	0.079822	1.00

0.1514	1.00		0.3817	1.00		1.97239	0.153027	P 10 1.0		
		P 1 1.0	0.1284	1.00		1.23883	-0.02562		23.87153	-0.000983
		P 1 1.0	0.0379	1.00		0.777	0.349601		14.92178	0.007129
		D 1 1.0	1.1168	1.00	P 1 1.0	0.2841	0.443888		9.32436	-0.031091
		D 1 1.0	0.325	1.00		0.1039	0.252695		5.82953	0.062401
		D 1 1.0	0.1024	1.00		0.777	1.00		3.15945	0.055414
		F 1 1.0	0.7649	1.00	P 1 1.0	0.2841	1.00		1.9749	0.028564
		F 1 1.0	0.2621	1.00		0.1039	1.00		1.2323	0.203529
					P 1 1.0	0.1039	1.00		0.508	0.369212
					P 1 1.0	0.0341	1.00	P 1 1.0	0.2094	0.366562
					D 1 1.0	1.893	1.00		0.0863	0.168151
					D 1 1.0	0.6679	1.00	P 1 1.0	1.2323	1.00
					D 1 1.0	0.2357	1.00	P 1 1.0	0.508	1.00
					D 1 1.0	0.0785	1.00	P 1 1.0	0.2094	1.00
					F 1 1.0	1.3632	1.00	P 1 1.0	0.0863	1.00
					F 1 1.0	0.4795	1.00	P 1 1.0	0.0305	1.00
					F 1 1.0	0.182	1.00	D 1 1.0	2.8558	1.00
					G 1 1.0	1.0059	1.00	D 1 1.0	1.1539	1.00
					G 1 1.0	0.4099	1.00	D 1 1.0	0.4663	1.00
								D 1 1.0	0.1884	1.00
								D 1 1.0	0.0689	1.00
								F 1 1.0	2.0768	1.00
								F 1 1.0	0.8737	1.00
								F 1 1.0	0.3676	1.00
								F 1 1.0	0.1432	1.00
								G 1 1.0	1.6787	1.00
								G 1 1.0	0.6752	1.00
								G 1 1.0	0.2976	1.00
								H 1 1.0	1.233	1.00
								H 1 1.0	0.5789	1.00

The energies and variances from VMC calculations on the water monomer with Hartree-Fock trial functions represented in terms of the aug-cc-pVXZ (CDF) basis sets and Casino Dirac-Fock pseudopotential employed on the O atom together with standard aug-cc-pVXZ basis sets being employed on the H atoms are reported in Table 7.5. Test calculations revealed that nearly the same energies and variances result when the pseudopotential and the aug-cc-pVXZ (CDF) basis sets are also employed on the H atoms. For this reason, in the remainder of the paper in

presenting results using GTO basis sets for the trial functions, the Casino Dirac-Fock pseudopotential and aug-cc-pVXZ (CDF) basis sets are used only for the O atoms. From Table 7.5, it is seen that with the aug-cc-pVDZ (CDF) basis set, the variance in the energy is reduced about threefold and the VMC energy is about 0.03 a.u. lower compared to the corresponding results obtained using the augmented BFD basis set on the O atom. With the aug-cc-pVTZ (CDF) basis set, the variance further is reduced to 0.29 au, which is very close to the value obtained with the plane-wave basis set with the 160 a.u. cutoff. For the largest GTO basis set considered, aug-cc-pV5Z (CDF), the variance is 0.22 a.u. As for the all-electron calculations, the results obtained with the larger GTO basis sets omitted the *g* and higher angular momentum functions from the O basis set and the *f* and higher angular momentum functions from the H basis set. However, given the fact that the energies and variances obtained with the aug-cc-pVTZ (CDF), and modified aug-cc-pVQZ (CDF) and aug-cc-pV5Z (CDF) basis sets are very close to those obtained with large cutoff plane-wave calculations, we conclude that the higher angular momentum functions are relatively unimportant for VMC calculations.

Table 7.5 VMC energies and variances for the water monomer^a

Basis set	VMC energy (a.u.)	Variance of the VMC energy (a.u.)
Aug-cc-pVDZ (CDF)	-17.193(2)	0.42
Aug-cc-pVTZ (CDF)	-17.197(1)	0.29
Aug-cc-pVQZ (CDF)	-17.199(1)	0.23
Aug-cc-pV5Z (CDF)	-17.200(1)	0.22

a. Results obtained employing a pseudopotential on the O atom only, with the standard aug-cc-pVXZ basis sets being used on the H atoms.

7.3 DMC CALCULATIONS

Figure 7.1 reports the results of DMC calculations on the water monomer with trial functions expanded in terms of the augmented BFD, the aug-cc-pVDZ (CDF), and aug-cc-pVTZ (CDF) GTO basis sets, as well as the 60 and 120 a.u. cutoff plane-wave basis sets. The DMC simulations were run using 10,000 walkers, about 35,000 Monte Carlo steps, and for time steps of 0.003, 0.005, 0.012, and 0.02 a.u., using the T-move procedure.^{173,174}

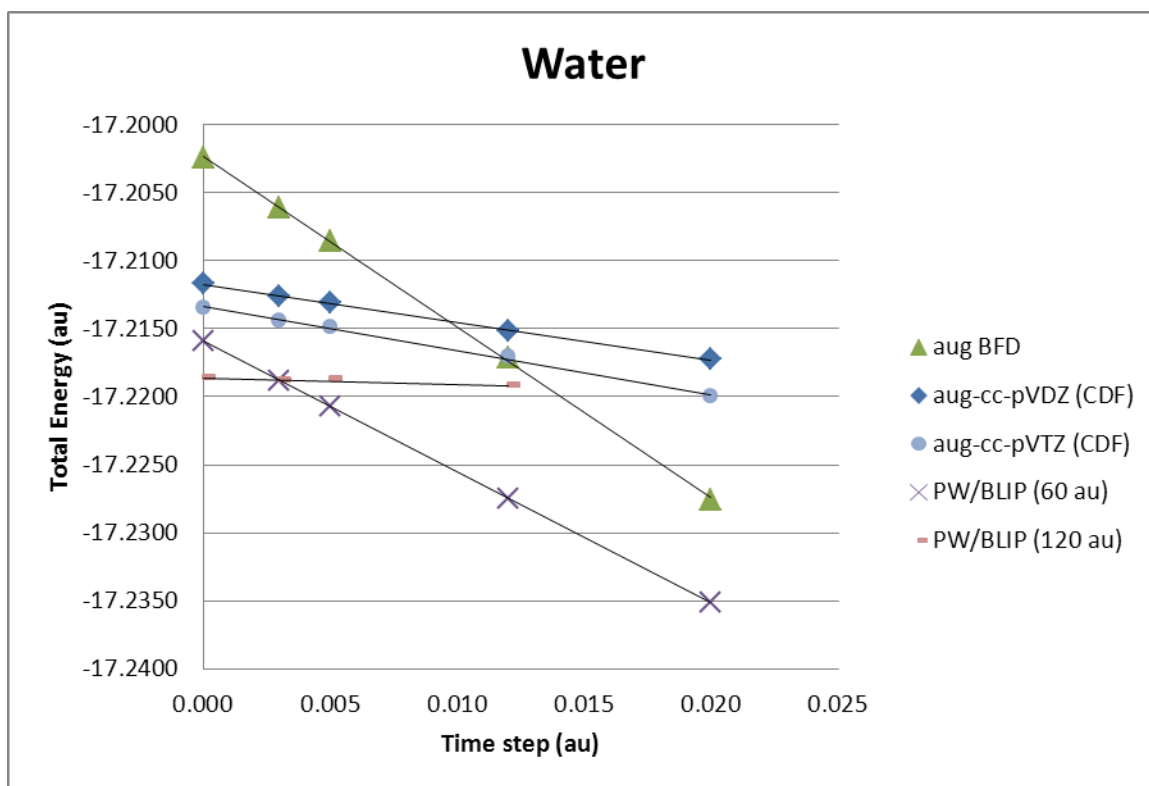


Figure 7.1 DMC energy of the water molecule with different trial functions

In each case the energies for the various time steps are well represented by linear fits, facilitating extrapolation to zero time step. Several trends are apparent from the data in this figure. First, DMC calculations using trial functions with the largest variances, namely those

expanded in terms of the augmented BFD and 60 a.u. cutoff plane-wave basis sets, display the large dependencies of the energies on the time step. Secondly, the DMC calculations with different trial functions give different total energies in the $t \rightarrow 0$ limit. The trial function using the augmented BFD basis set gives the highest DMC energy, -17.20207(9) a.u., and that represented in terms of plane-wave basis set with 120 a.u. cutoff, gives the lowest DMC energy, -17.2186(2). The calculations using the aug-cc-pVDZ (CDF) and aug-cc-pVTZ (CDF) basis sets give extrapolated DMC energies of -17.2117(1) and -17.21341(9), respectively. Of course, for typical applications, the relevant question is how the various methods perform at calculating energy differences. This will be examined below, where we report binding energies for the water dimer. However, before examining the binding energies we first consider the sensitivity of the total energies to the choice of the Jastrow factor and to the strategy, T-move^{173,174} or locality approximation (LA),¹⁷⁵ used to deal with errors introduced in the local approximation to the pseudopotential. Two different choices of the Jastrow factors are used, one obtained from a variance minimization and the other from an energy minimization.

In DMC calculations with pseudopotentials, the use of a non-local potential is incompatible with the fixed-node boundary condition, and the two schemes mentioned above can be used to deal with the problem. Each scheme has its advantages and disadvantages. The LA is believed to have smaller time step bias, but to have more stability problems.¹⁷⁶ In contrast, the T-move procedure is believed to be more stable with an additional advantage of being variational, but to require smaller time steps, especially for large systems.^{176,177}

We also calculated the binding energy of water dimer to determine whether the fact that different trial functions lead to different $t \rightarrow 0$ extrapolated total energies impacts the energy difference. Three different trial wave functions, HF with the aug-cc-pVTZ (CDF) basis sets, HF

with the augmented BFD basis set, and LDA with the plane-wave basis set (120 a.u. cutoff), were used in the calculations. The geometries of the water monomer and dimer were optimized at the MP2/aug-cc-pV5Z level. The optimized water dimer geometry has an equilibrium oxygen-oxygen distance of 2.9098 Å. The binding energy for each method was calculated by subtracting twice the energy of the monomer from the energy of the dimer.

Figure 7.2 reports the DMC total energies of water dimer obtained using different basis sets and the two approaches for dealing with the nonlocal pseudopotential problem. In each approach, two Jastrow factors were considered, one from variational minimization (Varmin) and the other from energy minimization (Emin). As expected, the DMC calculations with the augmented BFD basis set has the largest time step bias. Figure 7.3 shows on an expanded scale the DMC results with the aug-cc-pVTZ (CDF) basis set. Most significantly, it is seen that in the LA scheme the total DMC energy is more sensitive to the choice of Jastrow factor than when using the T-move procedure. With the LA procedure when used with the aug-cc-pVTZ (CDF) basis set, the two choices of Jastrow factors lead a difference of 0.5 kcal/mol in the total DMC energies in the zero time step limit. The difference is even greater when using the trial function represented in the plane-wave basis set. With the T-move scheme, the zero time step DMC energies obtained using the two Jastrow factors agree to each other within the error bars, even though the energy differences are significant at non-zero time steps. We were unable to perform a stable DMC calculation with the LA approach using the trial function represented in terms of the augmented BFD basis set, although such calculations ran smoothly with the aug-cc-pVTZ (CDF) basis set which was optimized for use with the Casino pseudopotential.

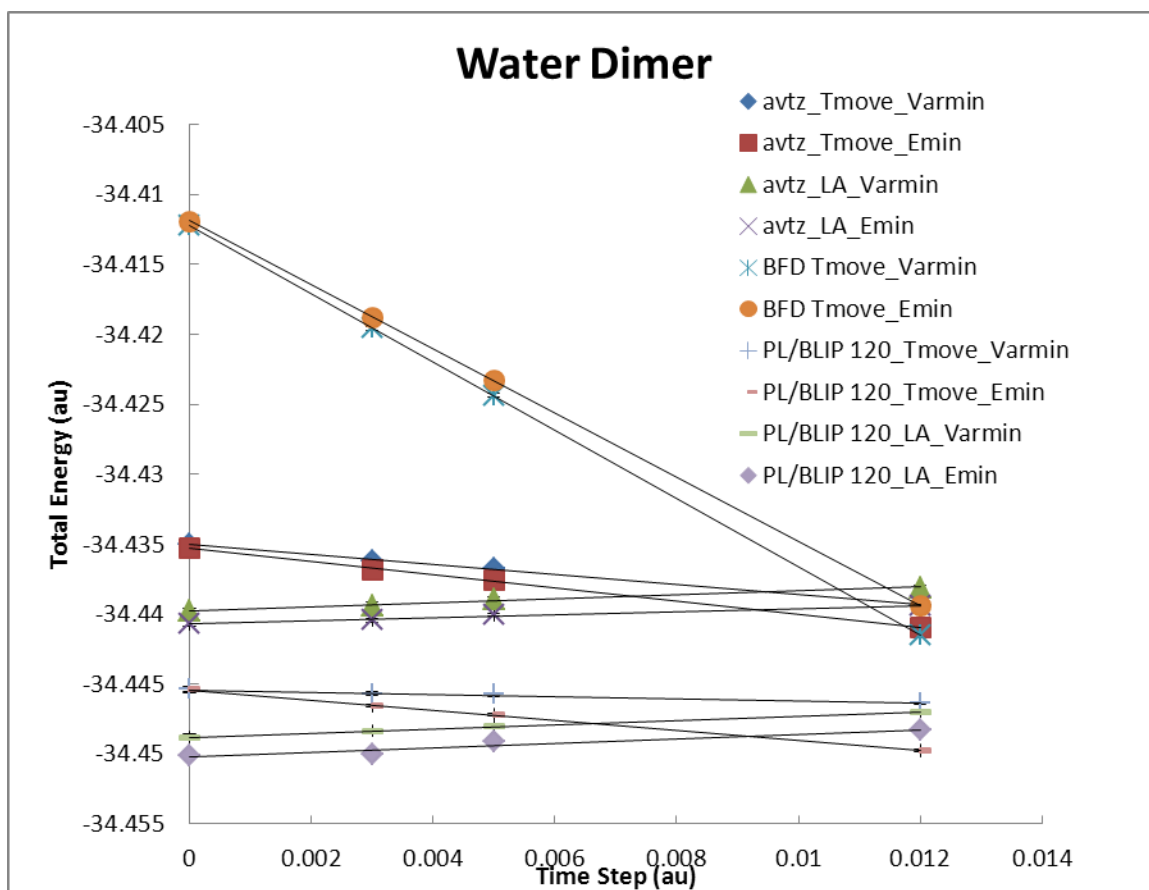


Figure 7.2 DMC energies of the water dimer obtained using different basis sets for representing the orbitals, different choices of Jastrow factors, and two strategies for dealing with the problems posed by non-local pseudopotentials

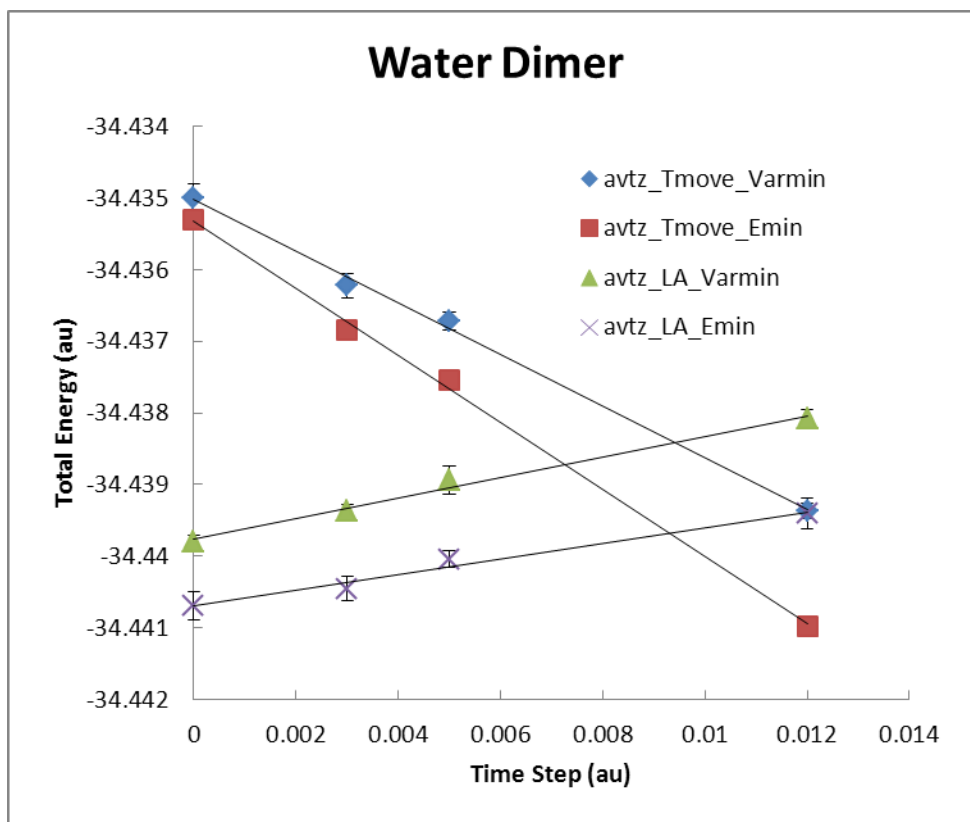


Figure 7.3 Energies of the water dimer on an expanded scale, from DMC calculations using the aug-cc-pVTZ (CDF) basis set

The DMC binding energies of water dimer obtained using HF orbitals expanded in terms of the aug-cc-pVTZ (CDF) GTO basis set, the augmented BFD basis set, and LDA orbitals expanded in terms of plane-wave basis set (120 a.u. cutoff) are reported in Table 7.6. The binding energy is calculated from the difference of the DMC energies of the water dimer and twice of the energies of the water monomer. As seen from Table 7.6, the DMC binding energies from the various approaches agree to each other within the error bars. They also agree with the DMC binding energies from prior all electron DMC calculations, as well as from complete-basis-set limit CCSD(T) calculations.^{37,72} Interestingly, even though the trial functions employing orbitals expanded in terms of the augmented BFD basis set have much larger variances in the VMC step and larger time step biases in the DMC step, they give, to within the statistical errors,

binding energies in agreement with those from the other calculations. However, one has to be cautious in generalizing this conclusion to more complex systems for which use of trial functions with large variance may prove more problematical for energy differences. Aside from these issues there is a decided efficiency advantage to using basis sets such as the aug-cc-pVXZ (CDF) basis sets introduced here, which are optimized for using with pseudopotentials used in quantum Monte Carlo calculations. For example, to achieve a specified statistical error in the DMC energy of the water dimer about half the computer time is required for the aug-cc-pVTZ (CDF) basis set than with the BFD basis set.

Table 7.6 Calculated binding energy of water dimer

Methods	Binding Energy (kcal/mol)
DMC/avtz_T-move_Varmin	-5.15±0.18
DMC/avtz_T-move_Emin	-5.06±0.08
DMC/avtz_LA_Varmin	-5.23±0.15
DMC/avtz_LA_Emin	-5.21±0.15
DMC/BFD_T-move_Varmin	-5.00±0.15
DMC/BFD_T-move_Emin	-5.06±0.15
DMC/PL/BLIP_120_T-move_Varmin	-5.15±0.18
DMC/PL/BLIP_120_T-move_Emin	-5.16±0.09
DMC/PL/BLIP_120_LA_Varmin	-5.16±0.18
DMC/PL/BLIP_120_LA_Emin	-5.03±0.14
DMC/HF ³⁷	-5.02±0.18
DMC/B3LYP ³⁷	-5.21±0.18
CCSD(T) CBS limit ⁷²	-5.02±0.05

In this paper, we also tested two strategies to obtain the binding energy. In the first strategy (S1) in Table 7.6, the binding energy is calculated from the difference of energy of the

water dimer and the sum of energies of two isolated water monomers. In the second strategy (S2), the energy of the water dimer at large separation is used in place of the sum of the energies of the two monomers. In the first case the energies of the individual species are extrapolated to the zero time step limit, and these extrapolated results are used to calculate the zero-time-step binding energies. In the second case, the zero-time-step binding energies were obtained by extrapolating the binding energies with different time steps. Although the final interaction energies obtained by extrapolation to zero-time steps should not depend on which strategy is used, we are interested in determining whether the errors due to the use of finite time steps largely cancel in the S2 strategy, as this would allow for a reduction in the computational effort.

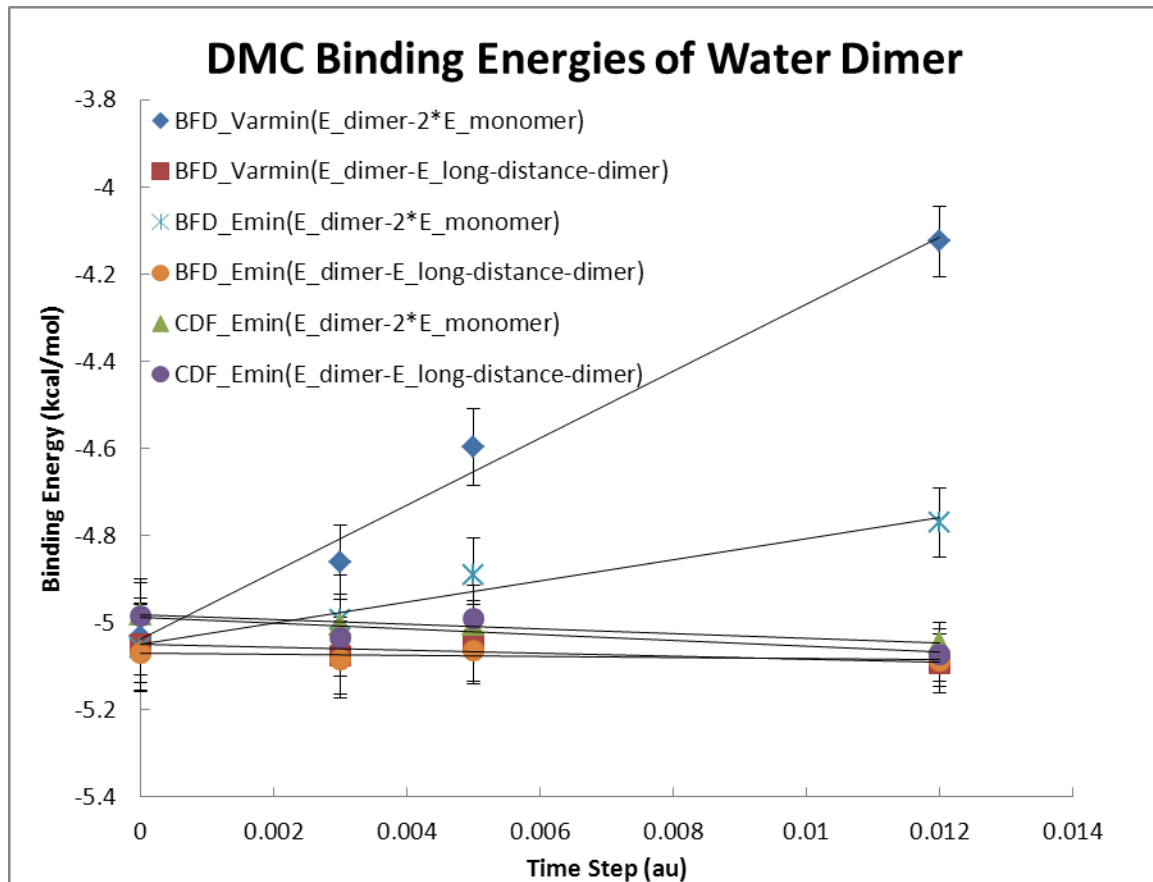


Figure 7.4 Binding energies of water dimer with two different trial functions and strategies

As shown in Figure 7.4, the extrapolated zero-time-step binding energies obtained using different trial functions and strategies are essentially identical. With the S1 procedure, there is large time step bias for the binding energy with the BFD basis set plus Casino Dirac-Fock pseudopotential, while most of the time step bias is cancelled when using CDF basis set plus Casino Dirac-Fock pseudopotential. In addition, in the cases with the S2 procedure applying both basis sets, most of the bias due to the use of finite time steps is removed from the result that, within the statistical errors, the same binding energy is obtained for each time step. This is most encouraging because it means that one can obtain accurate interaction energies by using the S2 procedure with only a single time step, no matter what the trial functions are applied. Moreover, a reasonably large value of the time step can be used reducing the computational time needed to achieve the desired convergence. With this approach, the computational effort can be reduced by about a factor of five compared to that required for the S1 procedure with the BFD basis set plus Casino Dirac-Fock pseudopotential.

7.4 CONCLUSIONS

In this work, we have developed for the C, O, and H atoms aug-cc-pVXZ (CDF) GOT basis sets for use with the Dirac-Fock pseudopotentials from the Needs group. These basis sets give greatly reduced variances compared to the GTO basis sets not designed for use with these pseudopotentials. This, in turn, leads to significantly improved convergence behavior in subsequent diffusion Monte Carlo calculations.

8.0 SUMMARY

In my dissertation research, I applied two particular variants of QMC, the variational Monte Carlo (VMC) and diffusion Monte Carlo (DMC) methods, to study several interesting and challenging electronic structure problems.

I carried out all-electron VMC and DMC calculations of the ground-state energy of the beryllium atom with single-determinant and multi-determinant trial functions. Beryllium is also challenging for the *ab initio* techniques because the near degeneracy of the 2s and 2p orbitals, significantly distorts the symmetry of the Be atom, and makes the RHF wave function a particularly poor choice. The resulting VMC energies with single-determinant trial functions with optimized Jastrow factors only recover about 60% of the correlation energy, while the VMC energy with a CASSCF trial function with optimized Jastrow factors recovers around 90% of the correlation energy. The DMC energies with all trial wave functions are at most 12 mHartree above the exact result of -14.667355(1) Hartree. The best DMC energy using a flexible CASSCF trial function with the CVB2 basis set is only 0.00006 Hartree above the exact energy, which is not only the best result in this study, but also the best DMC energy so far.

I performed all-electron VMC and DMC methods to calculate the total energy of the water monomer and dimer, and used these to calculate the binding energy D_e of the dimer. For the water monomer, the DMC total energy of water molecule with a HF trial function (DMC-HF) is only 24 mHartree above the exact result of -76.438 Hartree. The DMC binding energy with a

HF trial function agrees, within the statistical error, with the CCSD(T) and the MP2/CBS limit result.^{72,74}

I also used the DMC method with Hartree-Fock and Becke3LYP trial functions to calculate the electron binding energies of the $(\text{H}_2\text{O})_n^-$ cluster, obtaining results in excellent agreement with those of large basis set CCSD(T) calculations. Comparable quality CCSD(T) calculations would be feasible for $(\text{H}_2\text{O})_7^-$ and $(\text{H}_2\text{O})_8^-$ but would be computationally prohibitive for larger water clusters, due to its steep computational scaling. On the other hand, DMC calculations, with their N^3 (N is the number of electrons in the system) scaling and high degree of parallelization, should be applicable to $(\text{H}_2\text{O})_n^-$ clusters with n as large as 30.

The VMC and DMC methods have also been applied in the all-electron calculations of the binding energy of the water-benzene complex. The DMC dissociation energy matches very well with the MP2(CBS-limit) and CCSD(T)(CBS-limit) results¹¹⁵. Adding vibrational zero point energy (ZPE) corrections to our DMC electronic binding energy gives $\Delta E_0(0 \text{ K}) = -2.4 \pm 0.3$ kcal/mol, in good agreement with the experimental values of $\Delta E_0(0 \text{ K}) = -2.25 \pm 0.28$ kcal/mol¹¹⁶ and $\Delta E_0(0 \text{ K}) = -2.44 \pm 0.09$ kcal/mol.¹¹⁷

Pseudopotential QMC calculations have been performed to study the water-anthracene complex using Slater-Jastrow wave functions with Hartree-Fock single-particle orbitals. The resulting DMC binding energy agrees, within the error bars, with the results from Symmetry-Adapted Perturbation Theory (SAPT) and local MP2 (LMP2) methods with the aug-cc-pVTZ basis set.

It is also demonstrated that the DMC method using a Hartree-Fock trial function and the Casino Dirac-Fock pseudopotential gives binding energies for water-benzene and water-coronene that are consistent with the best prior estimates of these quantities from *ab initio*

calculations. It is found that the error due to the use of finite time steps can be mitigated by the use of a DMC calculation of the two monomers at large separation for obtaining the sum of the energies of the two non-interacting monomers. In light of this and the $O(N^3)$ scaling of DMC calculations, it would be possible to extend these calculations to water interacting with much larger acenes, such as hexabenzocoronene ($C_{42}H_{18}$) and circumcoronene ($C_{54}H_{18}$).

For large acene molecules, the DMC calculations with localized orbitals win out in the competition of the computational cost. However, the localized orbital method in Casino does not offer a huge advantage due to: (1) the current localization algorithm only localizing the σ orbitals correctly, forcing us to keep the π orbitals delocalized, and (2) the need to use larger localization radii for the larger acenes. In the future new algorithms to localize the π orbitals of π electron systems should be developed, which would greatly improve the scaling of DMC calculations on π electron systems.

Finally, newly designed correlation constant aug-cc-pVXZ (CDF) GTO basis sets have been applied in the DMC calculations with the Dirac-Fock pseudopotentials from the Needs' group. These basis sets give greatly reduced variances compared to the GTO basis sets not designed for use with these pseudopotentials. This, in turn, leads to significantly improved convergence behavior in subsequent diffusion Monte Carlo calculations.

QMC methods, such as VMC and DMC method, represent a powerful tool for finding solutions of the Schrödinger equation for atoms, molecules, and a variety of model systems. They are among the most accurate many-body methods for extended systems. Their intrinsically parallelizability makes them suitable for the current and next-generation massively parallel computers.

QMC methods are not only suitable for computing the energy of the interacting systems of electrons and fixed ions in the gas phase as described in this dissertation, but are also widely used in the condensed systems. Applications of the DMC to the electronic structure of solids include the properties of the homogeneous electron gas, cohesive energies of solids, equations of state, phase transitions, lattice defects, surface phenomena, and excited states.¹⁷⁸

Besides the VMC and DMC methods, other types of QMC methods are also increasingly being used in different research areas. For example, auxiliary field Quantum Monte Carlo (AFQMC) can be applied to treat excited states efficiently.¹⁷⁹ Path integral Monte Carlo (PIMC) is useful for high temperature electronic structure calculations and calculation of quantum properties involving light ions.¹⁸⁰ Coupled electron-ion Monte Carlo is good for low temperature properties, where one needs to go beyond methods based on density functional theory, particularly for disordered systems.¹⁸⁰

Trial wave functions play an important role in the QMC methods as they determine the accuracy of VMC results and provide the nodal surface for the DMC calculations. During recent years, significant progress has been made in using more sophisticated trial wave functions and in optimizing the parameters in them. Further advances are expected on this front.

In addition, force calculation in QMC methods is a topic of considerable research.¹⁸¹⁻¹⁸⁴ For example, a stochastic line-minimization algorithm relying on Bayesian inference was devised to find precise structural minima using energy estimates from accurate quantum Monte Carlo calculations.¹⁸⁵ Advances in this area will also stimulate progress in QMC-based dynamical methods. Molecular dynamics methods compatible with VMC and PIMC have been introduced by Miura.¹⁸⁶ QMC/MD calculations with QMC forces have also been carried out of liquid hydrogen to describe its properties under various thermodynamic conditions.¹⁸⁷

REFERENCE

- (1) Gervasio, F. L.; Chelli, R.; Procacci, P.; Schettino, V. *Proteins* **2002**, *48*, 117.
- (2) Liu, H.; Elstner, M.; Kaxiras, E.; Frauenheim, T.; Hermans, J.; Yang, W. *Proteins* **2001**, *44*, 484.
- (3) Appelbaum, I.; Wang, T.; Fan, S.; Joannopoulos, J. D.; Narayanamurti, V. *Nanotechnology* **2001**, *12*, 391.
- (4) Werder, T.; Walther, J. H.; Jaffe, R. L.; Halicioglu, T.; Koumoutsakos, P. *J. Phys. Chem. B* **2003**, *107*, 1345.
- (5) Sansom, M. S. P.; Biggin, P. C. *Nature* **2001**, *414*, 156.
- (6) Feller, D.; Jordan, K. D. *J. Phys. Chem. A* **2000**, *104*, 9971.
- (7) Gogotsi, Y.; Libera, J. A.; Gu v̇enc ü-Yazicioglu, A.; Megaridis, C. M. *Appl. Phys. Lett.* **2001**, *79*, 1021.
- (8) Bahr, J. L.; Mickelson, E. T.; Bronikowski, M. J.; Smalley, R. E.; Tour, J. M. *Chem. Commun.* **2001**, *2*, 193.
- (9) Jordan, K. D.; Johnson, M. A. *Science*, *329*, 42.
- (10) Diedrich, C.; Luchow, A.; Grimme, S. *J. Chem. Phys.* **2005**, *123*, 184106.
- (11) Tuckerman, M.; Laasonen, K.; Sprik, M.; Parinello, M. *J. Chem. Phys.* **1995**, *103*, 150.
- (12) Pati, R.; Zhang, Y.; Nayak, S. K.; Ajayan, P. M. *App. Phys. Lett.* **2002**, *81*, 2638.
- (13) Zhao, J.; Buldum, A.; Han, J.; Lu, J. P. *Nanotechnology* **2002**, *13*, 195.
- (14) Parr, R. G.; Yang, W. *Density-Functional Theory of Atoms and Molecules*; Oxford University Press: Oxford, 1989.
- (15) Allen, M.; Tozer, D. J. *J Chem Phys* **2002**, *117*, 11113.
- (16) Hobza, P.; Sponer, J.; Reschel, T. *J. Comput Chem* **1995**, *11*, 1315.

- (17) Kristyán, S.; Pulay, P. *Chem Phys Lett* **1994**, 229, 175.
- (18) Elstner, M.; Hobza, P.; Frauenheim, T.; Suhai, S.; Kaxiras, E. *J Chem Phys* **2001**, 114, 5149.
- (19) Zimmerli, U.; Parrinello, M.; Koumoutsakos, P. *J Chem Phys* **2004**, 120, 2693.
- (20) Grimme, S. *J Comput Chem* **2004**, 25, 1463.
- (21) Friesner, R. *Annu. Rev. Phys. Chem.* **1991**, 42, 34147.
- (22) Collins, P. G.; Bradley, K.; Ishigami, M.; Zettl, A. *Science* **2000**, 287, 1801.
- (23) Foulkes, W. M. C.; Mitas, L.; Needs, R. J.; Rajagopal, G. *Rev. Mod. Phys.* **2001**, 73, 33.
- (24) R.J. Needs; M.D. Towler; etc. **2007**.
- (25) Towler, M. *Phys. Stat. Sol. (b)* **2006**, 243, 2573.
- (26) Williamson, A. J.; Hood, R. Q.; Grossman, J. C. *Phys. Rev. Lett.* **2001**, 87, 246406.
- (27) Alfè D.; Gillan, M. J. *J. Phys.: Condens. Mater.* **2004**, 16, 305.
- (28) McMillan, W. L. *Phys. Rev.* **1965**, 138 A442.
- (29) Anderson, J. B. *J. Chem. Phys.* **1975**, 63, 1499.
- (30) Anderson, J. B. *J. Chem. Phys.* **1976**, 65, 4121.
- (31) Grimm, R. C.; Storer, R. G. *J. Comput. Phys.* **1971**, 7, 134.
- (32) Senatore, G., and N. H. March, . *Rev. Mod. Phys.* **1994**, 66, 445.
- (33) Ceperley, D. M. *Rev. Mod. Phys.* **1995a**, 67, 279.
- (34) Metropolis, N.; Rosenbluth, A. W.; Rosenbluth, M. N.; Teller, A. H.; Teller, E. *J. Chem. Phys.* **1953**, 21, 1087.
- (35) Feller, W. *An Introduction to Probability Theory and its Applications*; Wiley, New York, 1968; Vol. 1.
- (36) Hammond, B. L.; etc. *Monte Carlo methods in Ab Initio quantum chemistry*; World Scientific Publishing Co. Pte. Ltd., 1994.
- (37) Benedek, N. A.; Snook, I. K.; Towler, M. D.; Needs, R. J. *J. Chem. Phys.* **2006**, 125, 104302.
- (38) Reynolds, P. J.; Ceperley, D. M.; Alder, B. J.; and W. A. Lester, J. *J. Chem. Phys.* **1982**, 77, 5593.

- (39) Arnou, D. M.; Kalos, M. H.; Lee, M. A.; Schmidt, K. E. *J. Chem. Phys.* **1982**, *77*, 5562.
- (40) Ceperley, D. M.; Alder, B. J. *J. Chem. Phys.* **1984**, *81*, 5833.
- (41) Ceperley, D. M. *J. Stat. Phys.* **1991**, *63*, 1237.
- (42) Kato, T. *Communications on Pure and Applied Mathematics* **1957**, *10*, 151.
- (43) Jastrow, R. *J. Phys. Rev.* **1955**, *98*, 1479.
- (44) Drummond, N. D.; Towler, M. D.; Needs, R. J. *Phys. Rev. B* **2004**, *70*, 235119.
- (45) W. M. C. Foulkes; L. Mitas; R. J. Needs; G. Rajagopal. *Rev. Mod. Phys.* **2001**, *73*, 33.
- (46) C. E. Dykstra. *Chem. Phys. Lett.* **1977**, *45*, 466.
- (47) Handy, N. C.; Pople, J. A.; Head-Gordon, M.; Raghavachari, K.; Trucks, G. W. *chemical physics letters* **1989**, *164*, 185.
- (48) M. J. Frisch; G. W. Trucks; H. B. Schlegel; G. E. Scuseria; M. A. Robb; J. R. Cheeseman; J. A. Montgomery, Jr., T. V.; K. N. Kudin; J. C. Burant; J. M. Millam; S. S. Iyengar; J. Tomasi; V. Barone; B. Mennucci; M. Cossi; G. Scalmani; N. Rega; G. A. Petersson; H. Nakatsuji; M. Hada; M. Ehara; K. Toyota; R. Fukuda; J. Hasegawa; M. Ishida; T. Nakajima; Y. Honda; O. Kitao; H. Nakai; M. Klene; X. Li; J. E. Knox; H. P. Hratchian; J. B. Cross; V. Bakken; C. Adamo; J. Jaramillo; R. Gomperts; R. E. Stratmann; O. Yazyev; A. J. Austin; R. Cammi; C. Pomelli; J. W. Ochterski; P. Y. Ayala; K. Morokuma; G. A. Voth; P. Salvador; J. J. Dannenberg; V. G. Zakrzewski; S. Dapprich; A. D. Daniels; M. C. Strain; O. Farkas; D. K. Malick; A. D. Rabuck; K. Raghavachari; J. B. Foresman; J. V. Ortiz; Q. Cui; A. G. Baboul; S. Clifford; J. Cioslowski; B. B. Stefanov; G. Liu; A. Liashenko; P. Piskorz; I. Komaromi; R. L. Martin; D. J. Fox; T. Keith; M. A. Al-Laham; C. Y. Peng; A. Nanayakkara; M. Challacombe; P. M. W. Gill; B. Johnson; W. Chen; M. W. Wong; C. Gonzalez; J. A. Pople. Gaussian 03; Revision C.02 ed.; Gaussian, Inc.: Wallingford CT, 2004.
- (49) R. J. Needs; M. D. Towler; N. D. Drummond; P. López-Rós. CASINO version 2.1.0 User Manual; University of Cambridge: Cambridge, 2007.
- (50) Drummond, N. D.; R. J. Needs. *Phys. Rev. B* **2005**, *72*, 085124.
- (51) P. R. C. Kent; R. J. Needs; G. Rajagopal. *Phys. Rev. B* **1999**, *59*, 12344.
- (52) Martensson-Pendrill, A.; Alexander, S.; Adamowicz, L.; Oliphant, N.; Olsen, J.; Oster, P.; Quiney, H.; Salomonson, S.; Sundholm, D. *Phys. Rev. A* **1991**, *43*, 3355.
- (53) HARKLESS, J. A. W.; IRIKURA, K. K. *International Journal of Quantum Chemistry* **2006**, *106*, 2373.
- (54) Komasa, J.; Rychlewski, J.; Jankowski, K. *Phys Rev A* **2002**, *65*, 042507.

- (55) Ema, I.; Garcia De La Vega, J. M.; Ramirez, G.; Lopez, R.; Fernandez Rico, J.; Meissner, H.; Paldus, J. *J Comput Chem* **2003**, *24*, 859.
- (56) Van Lenthe, E.; Baerends, E. J. *J. Comput. Chem.* **2003**, *24*, 1142.
- (57) Toulouse, J.; Umrigar, C. J. *THE JOURNAL OF CHEMICAL PHYSICS* **2008**, *128*, 174101.
- (58) Park, C.-Y.; Kim, Y. *J. Chem. Phys.* **2001**, *115*, 2926.
- (59) Feller, D. *J. Chem. Phys* **1992**, *96*, 6104.
- (60) Tschumper, G. S.; Leininger, M. L.; Hoffman, B. C.; Valeev, E. F.; III, H. F. S.; Quack, M. *J. Chem. Phys.* **2002**, *116*, 690
- (61) Gurtubay, I. G.; Needs, R. J. *J. Chem. Phys.* **2007**, *127*, 124306.
- (62) Benedek, N. A.; Snooka, I. K.; Towler, M. D.; Needs, R. J. *J. Chem. Phys.* **2006**, *125*, 104302.
- (63) Mella, M.; Anderson, J. B. *J. Chem. Phys.* **2003**, *119*, 8225.
- (64) Kent, P. R. C.; Needs, R. J.; Rajagopal, G. *Phys. Rev. B* **1999**, *59*, 12344.
- (65) Needs, R. J.; Towler, M. D.; Drummond, N. D.; López-Rós, P. CASINO version 2.1.0 User Manual; University of Cambridge: Cambridge, 2007.
- (66) Benedict, W. S.; Gailar, N.; Plyler, E. K. *J. Chem. Phys.* **1956**, *24*, 1139.
- (67) Lüchow, A.; Anderson, J.; Feller, D. *J. Chem. Phys.*, *106*, 77061997.
- (68) Ermler, W.; Kern, C. *J. Chem. Phys.* **1974**, *61*, 3860.
- (69) Halkier, A.; Koch, H.; Jorgensen, P.; Christiansen, O.; Nielsen, I. M. B.; Helgaker, T. *Theor. Chem. Acc.* **1997**, *97*, 150.
- (70) Feller, D.; Boyle, C.; Davidson, E. *J. Chem. Phys.* **1987**, *86*, 3424.
- (71) Mas, E. M.; Bukowski, R.; Szalewicz, K.; Groenenboom, G. C.; Wormer, P. E. S.; Avoird, A. v. d. *J. Chem. Phys.* **2000**, *113*, 6687.
- (72) Klopper, W.; Rijdt, J. G. C. M. v. D.-v. d.; Duijneveldt, F. B. v. *Phys. Chem. Chem. Phys.* **2000**, *2*, 2227.
- (73) Diedrich, C.; Lüchow, A.; Grimme, a. S. *J. Chem. Phys.* **2005**, *123*, 184106.
- (74) Xantheas, S. S.; Burnham, C. J.; Harrison, R. J. *J. Chem. Phys.* **2002**, *116*, 1493.
- (75) Lee, H. M.; Suh, S. B.; Kim, K. S. *J. Chem. Phys.* **2003**, *118*, 9981.

- (76) Wang, F.; Jordan, K. D. *Annu. Rev. Phys. Chem.* **2003**, *54*, 367.
- (77) Pople, J. A.; Head-Gordon, M.; Raghavachari, K. *J. Chem. Phys.* **1987**, *10*, 5968.
- (78) Sommerfeld, T.; DeFusco, A.; Jordan, K. D. *J. Phys. Chem. A* **2008**, *112*, 11021.
- (79) Gutowski, M. unpublished results.
- (80) Herbert, J. M.; Head-Gordon, M. *J. Phys. Chem. A* **2005**, *109*, 5217.
- (81) Herbert, J. M.; Head-Gordon, M. *Phys. Chem. Chem. Phys.* **2006**, *8*, 68.
- (82) Williams, C. F.; Herbert, J. M. *J. Phys. Chem. A* **2008**, *112*, 6171.
- (83) Anderson, J. B. *J. Chem. Phys.* **1975**, *63*, 1499.
- (84) Anderson, J. B. *J. Chem. Phys.* **1976**, *65*, 4121.
- (85) Foulkes, W. M. C.; Mitas, L.; Needs, R. J.; Rajagopal, G. *Rev. Mod. Phys.* **2001**, *73*, 33.
- (86) Towler, M. D. *Phys. Status Solidi B* **2006**, *243*, 2573.
- (87) Hammer, N. I.; Shin, J. W.; Headrick, J. M.; Diken, E. G.; Roscioli, J. R.; Weddle, G. H.; Johnson, M. A. *Science* **2004**, *306*, 675.
- (88) Feng, D.-F.; Kevan, L. *Chem. Rev.* **1980**, *80*, 1.
- (89) Becke, A. D. *Phys. Rev. A* **1988**, *38*, 3098.
- (90) Becke, A. D. *J. Chem. Phys.* **1993**, *98*, 5648.
- (91) Lee, C.; Yang, W.; Parr, R. G. *Phys. Rev. B* **1988**, *37*, 785.
- (92) Stephens, P. J.; Devlin, F. J.; Chabalowski, C. F.; Frisch, M. J. *J. Phys. Chem.* **1994**, *98*, 11623.
- (93) Drummond, N. D.; Towler, M. D.; Needs, R. J. *Phys. Rev. B* **2004**, *70*, 235119.
- (94) McMillan, W. L. *Phys. Rev.* **1965**, *138*, 442.
- (95) Drummond, N. D.; Needs, R. J. *Phys. Rev. B* **2005**, *72*, 085124.
- (96) Umrigar, C. J.; Toulouse, J.; Filippi, C.; Sorella, S.; Hennig, R. G. *Phys. Rev. Lett.* **2007**, *98*, 110201.
- (97) Trail, J. R.; Needs, R. J. *J. Chem. Phys.* **2005**, *122*, 014112.
- (98) Trail, J. R.; Needs, R. J. *J. Chem. Phys.* **2005**, *122*, 174109.

- (99) Bergner, A.; Dolg, M.; Kuechle, W.; Stoll, H.; Preuss, H. *Mol. Phys.* **1993**, *80*, 1431.
- (100) Mella, M.; Anderson, J. B. *J. Chem. Phys.* **2003**, *119*, 8225.
- (101) Frisch, M. J.; Trucks, G. W.; Schlegel, H. B.; Scuseria, G. E.; Robb, M. A.; Cheeseman, J. R.; Montgomery, J., J. A.; Vreven, T.; Kudin, K. N.; Burant, J. C.; Millam, J. M.; Iyengar, S. S.; Tomasi, J.; Barone, V.; Mennucci, B.; Cossi, M.; Scalmani, G.; Rega, N.; Petersson, G. A.; Nakatsuji, H.; Hada, M.; Ehara, M.; Toyota, K.; Fukuda, R.; Hasegawa, J.; Ishida, M.; Nakajima, T.; Honda, Y.; Kitao, O.; Nakai, H.; Klene, M.; Li, X.; Knox, J. E.; Hratchian, H. P.; Cross, J. B.; Bakken, V.; Adamo, C.; Jaramillo, J.; Gomperts, R.; Stratmann, R. E.; Yazyev, O.; Austin, A. J.; Cammi, R.; Pomelli, C.; Ochterski, J. W.; Ayala, P. Y.; Morokuma, K.; Voth, G. A.; Salvador, P.; Dannenberg, J. J.; Zakrzewski, V. G.; Dapprich, S.; Daniels, A. D.; Strain, M. C.; Farkas, O.; Malick, D. K.; Rabuck, A. D.; Raghavachari, K. F., J. B.; Ortiz, J. V.; Cui, Q.; Baboul, A. G.; Clifford, S.; Cioslowski, J.; Stefanov, B. B.; Liu, G.; Liashenko, A.; Piskorz, P.; Komaromi, I.; Martin, R. L.; Fox, D. J.; Keith, T.; Al-Laham, M. A.; Peng, C. Y.; Nanayakkara, A.; Challacombe, M.; Gill, P. M. W.; Johnson, B.; Chen, W.; Wong, M. W.; Gonzalez, C.; and Pople, J. A.; . Gaussian03; Gaussian, Inc. : Wallingford CT 2004.
- (102) Needs, R. J.; Towler, M. D.; Drummond, N. D.; R ós, P. L. CASINO version 2.3 User Manual; University of Cambridge: Cambridge, 2008.
- (103) Dunning, T. H. J. *Journal of Chemical Physics* **1989**, *90*, 1007.
- (104) Xu, J.; Sommerfeld, T.; Jordan, K. D. *Unpublished results*.
- (105) Erlanger, B. F.; Chen, B.-X.; Zhu, M.; Brus, L. *Nano Lett.* **2001**, *1*, 465.
- (106) Huang, W.; Taylor, S.; Fu, K.; Lin, Y.; Zhang, D.; Hanks, T. W.; Rao, A. M.; Sun, Y.-P. *Nano Lett.* **2002**, *2*, 311.
- (107) Hunter, C. A. *J. Mol. Biol.* **1993**, *230*, 1025.
- (108) Li, S.; Cooper, V. R.; Thonhauser, T.; Puzder, A.; Langreth, D. C. *J. Phys. Chem. A* **2008**, *112*, 9031.
- (109) Suzuki, S.; Green, P. G.; Bumgarner, R. E.; Dasgupta, S.; Goddard, W. A., III; Blake, G. A. *Science* **1992**, *257*, 942.
- (110) Gutowsky, H. S.; Emilsson, T.; Arunan, E. *J. Chem. Phys.* **1993**, *99*, 4883.
- (111) Fredericks, S. Y.; Jordan, K. D. *J. Phys. Chem. A* **1996**, *100*, 7810.
- (112) Feller, D. *J. Phys. Chem. A* **1999**, *103*, 7558.
- (113) Tsuzuki, S.; Honda, K.; Uchimaru, T.; Mikami, M.; Tanabe, K. *J. Am. Chem. Soc.* **2000**, *122*, 11450.

- (114) Stoicheff, B. P. *Can. J. Phys.*, 1954, 339.
- (115) Jurecka, P.; Sponer, J.; Cerny, J.; Hobza, P. *Phys. Chem. Chem. Phys.* **2006**, 8, 1985.
- (116) Cheng, B.; Grover, J. R.; Walters, E. A. *Chem. Phys. Lett.* **1995**, 232, 364.
- (117) Courty, A.; Mons, M.; Dimicoli, I.; Piuze, F.; Gaigeot, M.; Brenner, V.; Pujol, P.; Millie, P. *J. Phys. Chem. A* **1998**, 102, 6590.
- (118) Drummond, N. D.; Rios, P. L.; Ma, A.; Trail, J. R.; Spink, G.; Towler, M. D.; Needs, R. *J. J. Chem. Phys.* **2006**, 124, 224104.
- (119) Trail, J. R.; Needs, R. *J. J. Chem. Phys.* **2005**, 122, 014112.
- (120) Trail, J. R.; Needs, R. *J. J. Chem. Phys.* **2005**, 122, 174109.
- (121) Gurtubay, I. G.; Drummond, N. D.; M. D. Towler; Needs, R. *J. J. Chem. Phys.* **2006**, 124, 024318
- (122) Jenness, G. R.; Jordan, K. *unpublished* **2007**.
- (123) Reyes, A.; Fomina, L.; Rumsh, L.; Fomine, S. *International Journal of Quantum Chemistry* **2005**, 104, 335.
- (124) Hernandez, E.; Gillan, M. J.; Goringe, C. M. *PHYSICAL REVIEW B* **1997**, 55, 13485.
- (125) Kysilka, J.; Rubes, M.; Grajciar, L.; Nachtigall, P.; Bludsky, O. *J. Phys. Chem. A* **2011**, 115, 11387.
- (126) Voloshina, E.; Usvyat, D.; Schutz, M.; Dedkov, Y.; Paulus, B. *Phys. Chem. Chem. Phys.* **2011**, 13, 12041.
- (127) Jenness, G. R.; Karalti, O.; Jordan, K. *Phys. Chem. Chem. Phys.* **2010**, 12, 6375.
- (128) Needs, R. J.; Towler, M. D.; Drummond, N. D.; Rios, P. L. *J. Phys.: Condens. Matter* **2010**, 22, 023201.
- (129) Nozieres, P.; Pines, D. *Phys. Rev.* **1958**, 111, 442.
- (130) Harl, J.; Kresse, G. *Phys. Rev. Lett.* **2009**, 103, 056401.
- (131) Lebegue, S.; Harl, J.; Gould, T.; Angyan, J. G.; Kresse, G.; Dobson, J. F. *Phys. Rev. Lett.* **2010**, 105, 196401.
- (132) Ma, J.; Michaelides, A.; Alfè, D.; Schimka, L.; Kresse, G.; Wang, E. *Phys. Rev. B* **2011**, 84, 033402.
- (133) Min, S. Y.; Lee, E. C.; Kim, D. Y.; Kim, D.; Kim, K. S. *J. Comput. Chem.* **2008**, 29, 1208.

- (134) Head-Gordon, M.; Pople, J. A.; Frisch, M. J. *Chem. Phys. Lett.* **1988**, *153*, 503.
- (135) Møller, C.; Plesset, M. S. *Phys. Rev.* **1934**, *46*, 618.
- (136) Deegan, M. J. O.; Knowles, P. J. *Chem. Phys. Lett.* **1994**, *227*, 321.
- (137) Hampel, C.; Peterson, K. A.; Werner, H.-J. *Chem. Phys. Lett.* **1992**, *190*, 1.
- (138) Raghavachari, K.; Trucks, G. W.; Pople, J. A.; Head-Gordon, M. *Chem. Phys. Lett.* **1989**, *157*, 479.
- (139) Boys, S. F.; Bernardi, F. *Mol. Phys.* **1970**, *19*, 553.
- (140) Misquitta, A. J.; Podeszwa, R.; Jeziorski, B.; Szalewicz, K. *J. Chem. Phys.* **2005**, *123*, 214103.
- (141) Hesselmann, A.; Jansen, G.; Schutz, M. *J. Chem. Phys.* **2005**, *122*, 014103.
- (142) Jeziorski, B.; Moszynski, R.; Szalewicz, K. *Chem. Rev.* **1994**, *94*, 1887.
- (143) Pitonak, M.; Hesselmann, A. *J. Chem. Theory Comput.* **2009**, *6*, 168.
- (144) Hesselmann, A. *J. Chem. Phys.* **2008**, *128*, 144112.
- (145) Xu, J.; Jordan, K. D. *J. Phys. Chem. A* **2009**, *114*, 1364.
- (146) Gurtubay, I. G. *J. Chem. Phys.* **2007**, *127*, 124306.
- (147) Ma, J.; Alfe, D.; Michaelides, A.; Wang, E. *J. Chem. Phys.* **2009**, *130*, 154303.
- (148) King, H. W. *CRC Handbook of Chemistry and Physics*, 2007.
- (149) Benedict, W. S.; Gailar, N.; Plyler, E. K. *J. Chem. Phys.* **1956**, *24*, 1139.
- (150) Courty, A.; Mons, M.; Dimicoli, I.; Piuze, F.; Gaigant, M.-P.; Breener, V.; Pujol, P. d.; Millie, P. *J. Phys. Chem. A* **1998**, *102*, 6590.
- (151) Rubes, M.; Nachtigall, P.; Vondrasek, J.; Bludsky, O. *J. Phys. Chem. C* **2009**, *113*, 8412.
- (152) Jenness, G. R.; Jordan, K. D. *J. Phys. Chem. C* **2009**, *113*, 10242.
- (153) Burkatzki, M.; Filippi, C.; Dolg, M. *J. Chem. Phys.* **2007**, *126*, 234105.
- (154) Kendall, R. A.; Dunning, T. H., Jr.; Harrison, R. J. *J. Chem. Phys.* **1992**, *96*, 6796.
- (155) Dunning, T. H., Jr. *J. Chem. Phys.* **1989**, *90*, 1007.
- (156) Janesko, B. G.; Henderson, T. M.; Scuseria, G. E. *J. Chem. Phys.* **2009**, *130*, 081105.

- (157) Perdew, J. P.; Burke, K.; Ernzerhof, M. *Phys. Rev. Lett.* **1996**, *77*, 3865.
- (158) Ren, X.; Tkatchenko, A.; Rinke, P.; Scheffler, M. *Phys. Rev. Lett.* **2011**, *106*, 153003.
- (159) Blum, V.; Gehrke, R.; Hanke, F.; Havu, P.; Havu, V.; Ren, X.; Reuter, K.; Scheffler, M. *Comput. Phys. Commun.* **2009**, *180*, 2175.
- (160) Havu, V.; Blum, V.; Havu, P.; Scheffler, M. *J. Comput. Phys.* **2009**, *228*, 8367.
- (161) Jenness, G. R.; Karalti, O.; Al-Saidi, W. A.; Jordan, K. D. *J. Phys. Chem. A* **2011**, *115*, 5955.
- (162) Jurecka, P.; Sponer, J.; Cerny, J.; Hobza, P. *Phys. Chem. Chem. Phys.* **2006**, *8*, 1985.
- (163) Feller, D. *J. Phys. Chem. A* **1999**, *103*, 7558.
- (164) Cheng, B. M.; Grover, J. R.; Walters, E. A. *Chem. Phys. Lett.* **1995**, 232.
- (165) Xu, J.; Jordan, K. D. *J. Phys. Chem. A* **2010**, *114*, 1364.
- (166) Xu, J.; Al-Saidi, W. A.; Jordan, K. D. *to be published*.
- (167) Alfè D.; Gillan, M. J. *Phys Rev B* **2004**, *70*, 161101.
- (168) Frisch, M. J.; Trucks, G. W.; Schlegel, H. B.; Scuseria, G. E.; Robb, M. A.; Cheeseman, J. R.; Montgomery, J. A., Jr., T. V.; Kudin, K. N.; Burant, J. C.; Millam, J. M.; Iyengar, S. S.; Tomasi, J.; Barone, V.; Mennucci, B.; Cossi, M.; Scalmani, G.; Rega, N.; Petersson, G. A.; Nakatsuji, H.; Hada, M.; Ehara, M.; Toyota, K.; Fukuda, R.; Hasegawa, J.; Ishida, M.; Nakajima, T.; Honda, Y.; Kitao, O.; Nakai, H.; Klene, M.; Li, X.; Knox, J. E.; Hratchian, H. P.; Cross, J. B.; Bakken, V.; Adamo, C.; Jaramillo, J.; Gomperts, R.; Stratmann, R. E.; Yazyev, O.; Austin, A. J.; Cammi, R.; Pomelli, C.; Ochterski, J. W.; Ayala, P. Y.; Morokuma, K.; Voth, G. A.; Salvador, P.; Dannenberg, J. J.; Zakrzewski, V. G.; Dapprich, S.; Daniels, A. D.; Strain, M. C.; Farkas, O.; Malick, D. K.; Rabuck, A. D.; Raghavachari, K.; Foresman, J. B.; Ortiz, J. V.; Cui, Q.; Baboul, A. G.; Clifford, S.; Cioslowski, J.; Stefanov, B. B.; Liu, G.; Liashenko, A.; Piskorz, P.; Komaromi, I.; Martin, R. L.; Fox, D. J.; Keith, T.; Al-Laham, M. A.; Peng, C. Y.; Nanayakkara, A.; Challacombe, M.; Gill, P. M. W.; Johnson, B.; Chen, W.; Wong, M. W.; Gonzalez, C.; Pople, J. A. Gaussian 03; Revision C.02 ed.; Gaussian, Inc.: Wallingford CT, 2004.
- (169) Gonze, X.; Amadon, B.; Anglade, P. M.; Beuken, J. M.; Bottin, F.; Boulanger, P.; Bruneval, F.; Caliste, D.; Caracas, R.; Deutsch, T.; Genovese, L.; Ghosez, P.; Giantomassi, M.; Goedecker, S.; Hamann, D. R.; Hermet, P.; Jollet, F.; Jomard, G.; Leroux, S.; Mancini, M.; Mazevet, S.; Oliveira, M. J. T.; Onida, G.; Pouillon, Y.; Rangel, T.; Rignanese, G. M.; Sangalli, D.; Shaltaf, R.; Torrent, M.; Verstraete, M. J.; Zerah, G.; Zwanziger, J. W. *Comput. Phys. Commun.* **2009**, *180*, 2582.
- (170) Peterson, K. A. *THE JOURNAL OF CHEMICAL PHYSICS* **2003**, *119*, 11099.

- (171) Peterson, K. A.; Figgen, D.; Goll, E.; Stoll, H.; Dolg, M. *THE JOURNAL OF CHEMICAL PHYSICS* **2003**, *119*, 11113.
- (172) Peterson, K. A.; Shepler, B. C.; Figgen, D.; Stoll, H. *The Journal of Physical Chemistry A* **2006**, *110*, 13877.
- (173) Casula, M.; Filippi, C.; Sorella, S. *Phys. Rev. Lett.* **2005**, *95*, 100201.
- (174) Casula, M. *Phys. Rev. B* **2006**, *74*, 161102.
- (175) Mitas, L.; Shirley, E. L.; Ceperley, D. M. *THE JOURNAL OF CHEMICAL PHYSICS* **1991**, *95*, 3467.
- (176) Needs, R. J.; Towler, M. D.; Drummond, N. D.; Ros, P. L. *J. Phys.: Condens. Matter* **2010**, *22*, 023201.
- (177) Casula, M.; Moroni, S.; Sorella, S.; Filippi, C. *THE JOURNAL OF CHEMICAL PHYSICS*, *132*, 154113.
- (178) Koloren, J.; Mitas, L. *Rep. Prog. Phys.* **2011**, *74*, 026502.
- (179) Fayton, F. A.; Gibson, A. A.; Harkless, J. A. W. *Int. J. Quantum Chem* **2009**, *109*, 43.
- (180) Ceperley, D. M. *Reviews in Mineralogy and Geochemistry* **2010**, *71*, 129.
- (181) Badinski, A.; Haynes, P. D.; Needs, R. J. *Phys. Rev. B* **2008**, *77*, 085111.
- (182) Badinski, A.; Trail, J. R.; Needs, R. J. *J. Chem. Phys.* **2008**, *129*, 224101.
- (183) Austin, B. M.; Zubarev, D. Y.; Lester, W. A. *Chem. Rev.* **2012**, *112*, 263.
- (184) Badinski, A.; Needs, R. J. *Phys. Rev. B* **2008**, *78*, 035134.
- (185) Wagner, L. K.; Grossman, J. C. *Phys. Rev. Lett.* **2010**, *104*, 210201.
- (186) Miura, S. Molecular Dynamics and Hybrid Monte Carlo Algorithms for the Variational Path Integral with a Fourth-Order Propagator. In *Advances in Quantum Monte Carlo*; American Chemical Society, 2012; Vol. 1094; pp 177.
- (187) Attaccalite, C.; Sorella, S. *Phys Rev Lett* **2008**, *100*, 17.